Hepatocyte-intrinsic SMN deficiency drives metabolic dysfunction and liver steatosis in spinal muscular atrophy
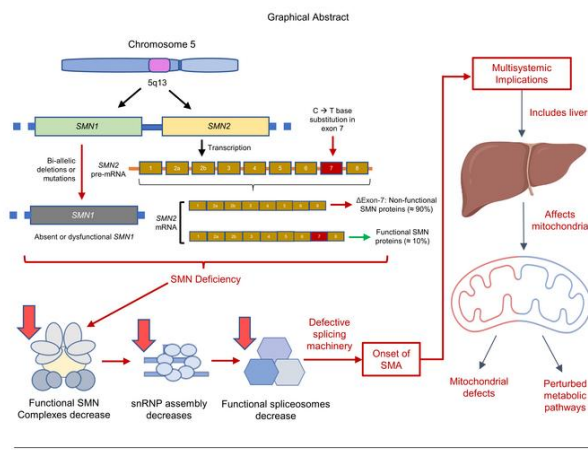
Damien Meng-Kiat Leow, … , Basil T. Darras, Crystal J.J. Yeo

Research In-Press Preview Metabolism Neuroscience

Graphical abstract

Graphical abstract. Portions of the figures created with BioRender.com.

Find the latest version:

https://jci.me/173702/pdf

Hepatocyte-intrinsic SMN deficiency drives metabolic dysfunction and liver steatosis in spinal muscular atrophy

Damien Meng Kiat Leow[#, 1], Yang Kai Ng[#, 1, 2], Loo Chien Wang[2], Hiromi W. L. Koh[2], Tianyun Zhao[2], Zi Jian Khong[2], Tommasco Tabaglio[2], Gunaseelan Narayanan[3], Richard M. Giadone[4], Radoslaw M. Sobota[2], Shi Yan Ng[1, 2, 5], Adrian Kee Keong Teo[1, 2], Simon H. Parson[6], Lee L. Rubin[4], Wei Yi Ong [1], Basil T. Darras[7], Crystal J. J. Yeo[*2,3, 5-9]

[#]co-first authors

*Corresponding author: Crystal J. J. Yeo

Address:

Translational Neuromuscular Medicine Laboratory, Institute of Molecular and Cell Biology, Agency for Science, Technology and Research (A*STAR), 61 Biopolis Drive, Proteos, Singapore 138673, Republic of Singapore

Phone number: +65 68569547

Email: crystaljjyeo@cantab.net

[1] Yong Loo Lin School of Medicine, National University of Singapore, Singapore 117597, Republic of Singapore

[2] Institute of Molecular and Cell Biology (IMCB), Agency for Science, Technology and Research (A*STAR), 61 Biopolis Drive, Proteos, Singapore 138673, Republic of Singapore

[3] Duke-NUS Medical School, Singapore 169857, Republic of Singapore

[4] Department of Stem Cell and Regenerative Biology, Harvard University, Cambridge MA 02138, USA

[5] National Neuroscience Institute, Singapore 308433, Republic of Singapore.

[6] Institute of Education in Healthcare and Medical Sciences, School of Medicine, Medical Sciences and Nutrition, University of Aberdeen, Aberdeen, AB51 7HA, Scotland

[7] Department of Neurology, Boston Children's Hospital, Harvard Medical School, Boston, Massachusetts, USA.

[8] Department of Neurology, Feinberg School of Medicine, Northwestern University, Chicago, IL, USA.

[9] Lee Kong Chian School of Medicine, Nanyang Technological University, Singapore 308232, Republic of Singapore.

Abstract

Spinal Muscular Atrophy (SMA) is typically characterized as a motor neuron disease, but extra-neuronal phenotypes are present in almost every organ in severely affected patients and animal models. Extra-neuronal phenotypes were previously underappreciated as patients with severe SMA phenotypes usually died in infancy; however, with current treatments for motor neurons increasing patient lifespan, impaired function of peripheral organs may develop into significant future comorbidities and lead to new treatment-modified phenotypes. Fatty liver is seen in SMA animal models , but generalizability to patients and whether this is due to hepatocyte-intrinsic Survival Motor Neuron (SMN) protein deficiency and/or subsequent to skeletal muscle denervation is unknown. If liver pathology in SMA is SMN-dependent and hepatocyte-intrinsic, this suggests SMN repleting therapies must target extra-neuronal tissues and motor neurons for optimal patient outcome. Here we showed that fatty liver is present in SMA and that SMA patient-specific iHeps were susceptible to steatosis. Using proteomics, functional studies and CRISPR/Cas9 gene editing, we confirmed that fatty liver in SMA is a primary SMN-dependent hepatocyte-intrinsic liver defect associated with mitochondrial and other hepatic metabolism implications. These pathologies require monitoring and indicate need for systematic clinical surveillance and additional and/or combinatorial therapies to ensure continued SMA patient health.

Introduction

Spinal Muscular Atrophy (SMA) is one of the most common monogenetic autosomal recessive neuromuscular genetic diseases, with a worldwide carrier frequency of approximately 1/52 and disease incidence around 1/10,000 [1]. SMA clinical phenotypes are heterogenous, ranging from infanthood to adulthood, and classified into five major types based on age at onset of symptoms and maximum level of motor function achieved [2-6], with the most severe being SMA Types 0 and 1, and mildest being SMA Types 3-4. The disease is caused by biallelic deletions in *Survival Motor Neuron 1* (*SMN1)* genes [7], resulting in a scarcity of Survival Motor Neuron (SMN) protein and death of motor neurons. One to more than four copies of *Survival Motor Neuron 2* (*SMN2*) gene, a highly homologous version of *SMN1,* are present in 95% of humans [8], and a c.840 C>T transition in exon 7, which converts an Exonic Splicing

Enhancer into an Exonic Splicing Silencer, causes aberrant splicing and production of mostly truncated SMN protein [9]. Fewer *SMN2* copies and lower amounts of SMN protein are associated with the most severe phenotypes (SMA Type 0 and Type 1).

Before the Federal Drug Agency's (FDA) approval of anti-sense oligonucleotide (ASO) nusinersen in 2016 [10], adeno-associated virus serotype 9-mediated *SMN1* gene replacement therapy onasemnogene abeparvovec-xioi in 2019 [11], and small molecule splicing *SMN2* modifier risdiplam in 2020 [12], SMA was invariably fatal in infancy for the most severe forms of SMA. With recent innovative advances in the therapeutic landscape, infants and children below age of two with SMA Type 1 can now survive to childhood [10, 13] and are expected to survive into adulthood. It is thought that they are unlikely to achieve full motor capacity as these new therapeutics are not outright cures. These therapeutics can only increase full-length functional SMN protein expression to halt the progression of disease by preventing future motor neuron loss, but cannot reverse motor neuron loss which has already occurred. Additionally, data is still emerging concerning treatment tolerability, efficacy and durability in different clinical settings and age groups, and the long-term adverse effects of treatment are unclear [14].

While SMA is typically characterized as a motor neuron disease, extra-neuronal phenotypes have been noted in severely affected patients and animal models [15]. Data from autopsies, case studies and limited cohort studies in patients with severe SMA correspond with animal models of SMA, showing dysfunction in almost every peripheral organ system, including the skeletal muscle, heart, kidney, liver, pancreas, spleen, bone, connective tissues and immune systems, providing evidence in support of SMA as a multi-system disorder [16-19]. SMN protein is ubiquitously expressed in all tissues and has roles in ribonucleoprotein components, RNA transcription and splicing [20], ribosomal function and messenger RNA translation, however the complete range of functions of SMN protein in all tissues is unknown [21, 22]. Extra-neuronal phenotypes were not a focus in the past as patients with severe phenotypes of SMA usually died by the age of two years, but with current treatments which increase survival and lifespans of SMA patients, impaired function of peripheral tissues and organs may become significant future comorbidities and cause the emergence of treatment-modified phenotypes, particularly for treatments which only target motor neurons [14]. It is vital to understand extra-neuronal phenotypes to inform systematic clinical surveillance and treatment programs. Whether extra-neuronal phenotypes are caused by cell-intrinsic SMN protein deficiency and/or secondary to motor neuron death, needs to be explored as it changes patient management. In

the former, SMN repleting therapies must target extra-neuronal tissues as well as motor neurons for optimal treatment outcome; in the latter, treatment of motor neurons would suffice.

The liver is an important organ to study in SMA because of its many functions in detoxification, metabolism, immune regulation, hematopoiesis and clotting [23], and its implications for SMA treatments. Onasemnogene abeparvovec-xio is usually associated with mild to moderate hepatotoxicity within days to a few weeks of treatment [13]. Notably, in August 2022, two children with SMA died of acute liver failure 6-7 weeks after receiving gene therapy, suggesting an urgent need to identify patients who react poorly to treatment and to understand the mechanisms underlying liver damage in SMA [24]. Risdiplam is primarily metabolized by hepatic Flavin Monooxygenases 1 and 3 (FMO1 and FMO3) [25], and changes in pharmacokinetics may affect drug efficacy, durability and toxicity. Over 5000 hepatic genes are dysregulated with disease progression in mouse models of SMA, as compared to 1000 genes in muscle, suggesting that despite SMA being classified as a neuromuscular disease, pathways are also significantly dysregulated in the liver [26]. Targeted hepatic ablation of SMN is embryonically lethal [27] and peripheral depletion of SMN in adult mice results in lipid accumulation, altered iron homeostasis [28], hepatocellular necrosis and inflammatory infiltrates [29]. Animal models of SMA have fatty liver, but it is not known whether this is primarily due to hepatic SMN deficiency or secondary to metabolic changes subsequent to skeletal muscle denervation [30, 31]. The etiology, importance, and generalizability of these findings to patients with SMA remain unclear; although one small study showed hepatic steatosis in a proportion of necropsies of patients diagnosed with SMA, most of the diagnoses were obtained through clinical examination and histology prior to the era of genetic testing [30].

The primary goal of this study was to describe hepatic defects in SMA patients and cell-intrinsic defects in SMA patient-derived induced pluripotent stem cell (iPSC)-derived hepatocyte-like cells (iHeps). We retrospectively analyzed clinical data from a single center cohort of pediatric and adult SMA patients without liver disease who received hepatic sonography. Sonographic steatosis grade and serum markers of liver function were reviewed as potential clinical biomarkers of liver dysfunction. In parallel, we differentiated Type 0 to Type 3 SMA patient iPSCs into iHeps to evaluate SMA hepatocyte-intrinsic effects. Lipid accumulation and proteomics were analyzed. We CRISPR-edited a c.840 T>C transition in exon 7 of *SMN2* to generate *SMN1*-like genes with full-length SMN protein expression in a SMA Type 1 iPSC line to rescue SMN protein expression on an isogenic background and

confirm SMN-dependent effects. This work demonstrates that SMA patient hepatic steatosis is a cell-intrinsic metabolic phenotype, and highlights the critical need for further investigation of the liver in SMA and its clinical implications.

Results

<Table 1>

SMA Patients Display Liver Steatosis

Liver pathology, and specifically fatty liver (steatosis), have been described in mouse models of SMA, but patient data in this area is scant. To examine if steatosis is present in the patient population, we carried out a retrospective, single-center cohort study on pediatric and adult patients with SMA Types 1-3 who had undergone liver ultrasound and collection of clinical serum markers of liver function. All patients were on risdiplam, nusinersen or had received gene therapy. 6/8 (75%) of these SMA patients had ultrasonic evidence of increased hepatic echogenicity consistent with mild to moderate hepatic steatosis. 3/8 (37.5%) also had deranged serum markers indicative of liver damage, namely elevations of alanine transaminase (ALT), aspartate transaminase (AST) and gamma glutamyl transferase (GGT) (**Table 1**). One of the patients who had elevated GGT without increased hepatic echogenicity was taking phenobarbital, a drug that can cause hepatocellular damage. Two adults with SMA had possible non-SMA causes of liver dysfunction: obesity and heavy alcohol use. None had alterations in clinical serum markers of protein synthetic function (Albumin, Protein, Bilirubin) and only the patient with obesity had impaired fasting glucose suggestive of insulin resistance. Interestingly, we found that hepatic steatosis was detected in patients across all SMA genotypes examined, regardless of severity of the neuromuscular phenotype. Increased hepatic echogenicity therefore has potential as a non-invasive and sensitive biomarker for a range of SMA types, although care should be taken to exclude other causes of liver dysfunction. Interestingly, steatosis is present in treated patients, suggesting that current therapies may not be sufficient to target this phenotype for these patients at the time of treatment.

SMA iHeps Show Increased Lipid Accumulation

To determine if the pathological liver phenotype seen in SMA patients was hepatocyte-intrinsic, we created an *in-vitro* hepatocyte model. To do this, we differentiated SMA and non-

SMA (WT) human iPSCs into iHeps [32, 33], as an *in vitro* model of the SMA liver phenotype (**Supplementary Fig. S1**). SMA iPSCs were obtained from untreated SMA patients. D24 iHeps displayed large angular polygonal morphology, distinct round nuclei with one or two prominent nucleoli and binucleate cells with bright junctions, characteristic of mature hepatocytes (**Supplementary Fig. S1**). Quality control for qRT-PCR primers and house-keeping genes were performed prior to gene analysis (**Supplementary Fig. S2**). qRT-PCR showed expression of a range of liver-specific genes: albumin (*ALB*), asialoglycoprotein receptor 1 (*ASGR1*) and 2 (*ASGR2*), apolipoprotein E (*APOE*), apolipoprotein A1 (*APOA1*), prothrombin (*F2*), α1-antitrypsin (*SERPINA1*), haptoglobin (*HP*), hepatocyte nuclear factor 4 alpha (*HNF4A*), and alpha-fetoprotein (*AFP*), representing liver-specific functions of serum protein secretion and homeostasis, lipid metabolism, clotting, and hemolysis (**Supplementary Fig. S3A & S4A**). Conversely, gene expression of embryonic stem cell markers, POU class 5 homeobox 1 (*OCT4*), nanog homeobox (*NANOG*) and SRY-box transcription factor 2 (*SOX2*) were negligible(**Supplementary Fig. S3B & S4B**). The iHeps were determined to be functional as we found similar levels of urea secretion in cultures of WT and SMA Type 1 (SMA1) and SMA Type 3 (SMA3) iHeps (**Supplementary Fig. S3C**).

< Figure 1 & 2>

Consistent with SMA pathology, SMA iHeps showed markedly reduced SMN protein expression on Western Blot and image analysis (**Fig. 1A-B**). Patient-derived SMA iHeps had increased numbers of small and large vacuoles, (**Fig. 1C**) which stained with Oil Red O (ORO), the gold standard histochemical stain for identifying lipids (**Fig. 2A**). Using ORO and image analysis to quantify steatosis [34], SMA iHeps showed 10-fold increase in lipid accumulation compared to WT (**Fig. 2B**). Mean ORO staining intensity per 50 cells in each line is presented in **Supplementary Fig. S5A**. Normalisation of mean ORO staining intensity to cell number is presented in **Supplementary Fig. S5C**. Lipid accumulation was similar across mild (SMA3) and severe (SMA1) clinical phenotypes, which showed that lipid accumulation is hepatocyte-intrinsic and present across a range of untreated SMA severities.

Distinct Proteome Alterations Are Present in SMA iHeps

< Figure 3 & 4>

We next assessed protein pathways affected in SMA iHeps. For an overview of changes in the entire proteome in liver of SMA patients, SMA Types 0-3 and WT iHeps were subjected to

quantitative proteome analysis. From the 657 proteins differentially expressed in at least one of the SMA phenotypes compared to WT, we identified 343 proteins which also exhibited trends correlating with disease severity. To understand their roles in the liver, we performed a STITCH and K-means clustering analysis, which identifies interaction networks between proteins and Gene Ontology (GO) enrichment analysis to identify potential biological processes. Resulting three clusters of affected protein networks (**Fig. 3A**) indicate processes related to mitochondrial pathways and lipid metabolism, golgi and endoplasmic reticulum (ER) transport and protein synthesis were all dysregulated in SMA iHeps (**Supplementary Fig. S6 – S12**), with overall downregulation of proteins involved in oxidative phosphorylation, lipid metabolism, and golgi/ER related transport, and upregulation of proteins involved in protein synthesis (**Fig. 3B-D**).

To further understand how mitochondrial dysfunction and lipid homeostasis may influence hepatic steatosis in SMA, we performed an in-depth analysis of dysregulated proteins related to mitochondrial processes and lipid homeostasis using GO methodology (**Supplementary Fig. S9 and S11**). Top GO terms generated included "Mitochondrial ATP synthesis coupled proton transport", "ATP biosynthetic process", "Cholesterol metabolism" and "Fatty acid metabolism" (**Supplementary Fig. S9C and S11B**). 54 protein hits matched to the MitoCarta3.0 mitochondrial protein and pathway inventory. Most strikingly, mitochondrial proteins involved in mitochondrial protein translation and ribosomal complex were found to be upregulated whereas several ATP complex V subunits were downregulated (**Fig. 4A**). Top Mitopathways affected were "Metabolism", "Small molecule transport", "Mitochondrial central dogma", "OXPHOS" and "Mitochondrial signalling"(**Supplementary Fig. S10**). In addition, specific proteins associated with lipid transport (APOA1) and fatty acid oxidation (ACAD11) were downregulated and positively correlated with increasing SMA severity. The converse was true for proteins associated with cholesterol synthesis (HMGCS1) and triglyceride accumulation (ACAT2), which were upregulated (**Fig. 4B-C**). These findings suggest that mitochondrial dysfunction and lipid metabolism may contribute to the observed SMA liver phenotype.

SMA iHeps show Metabolic Dysfunction

< Figure 5>

Since dysregulation of mitochondrial ATP synthesis was implicated as an important disease pathway in the SMA liver phenotype, we tested if mitochondrial bioenergetics were

compromised in SMA1 iHeps using mitochondrial respirometry [35]. Mitochondrial oxygen consumption rate (OCR) of WT and SMA Type 1 iHeps was tested using a Seahorse analyser and showed impairment of mitochondrial bioenergetics in SMA iHeps across multiple indicators (**Fig. 5A-G**), including ATP-linked respiration (**Fig. 5C**). We then performed cellular metabolic assays on WT and SMA iHeps and showed that SMA iHeps had reduced intracellular ATP (**Fig. 5H**) and succinate dehydrogenase activity using MTT assay (**Fig. 5I**). Defective mitochondrial respiration and ATP production can lead to increased mitochondrial oxidative stress [36] and compromised mitochondrial membrane potential (MMP) [37]. SMA iHeps showed a decrease in MMP (**Supplementary Fig. S14**) and an associated increase in mROS production (**Fig. 5J**). Mitochondria have an important role in buffering intracellular calcium, which is dysregulated in SMA astrocytes [38], SMA cardiomyocytes [39], SMA neurons [40] and Amyotrophic Lateral Sclerosis (ALS), another motor neuron disease [41]. However, we found no difference in intracellular calcium levels in SMA iHeps compared to WT (**Fig. 5K**), suggesting that mitochondrial defects in SMA iHeps might not be mediated through calcium dependent pathways [42]. These findings show that multiple indicators of metabolic dysfunction are present in SMA iHeps.

SMA iHeps Show Dysregulation of Genes implicated in Mitochondrial Function, Metabolism and Hepatic Function, and Critical Proteins involved in Mitochondrial Electron Transport Chain and Fatty Acid Oxidation.

< Figure 6 & 7>

Since SMN regulates gene transcription [43], we evaluated the expression of genes related to the alterations in proteome analysis initially generated (**Fig. 3& 4**). We hypothesized that genes relating to metabolism and hepatic function, previously identified, may also be affected (**Supplementary Fig. S3A & S4A**).

Genes coding for proteins involved in mitochondrial Oxidative Phosphorylation (OXPHOS) - succinate dehydrogenase complex flavoprotein subunits A, B, and C (*SDHA*, *SDHB*, and *SDHC* respectively code for proteins in Complex II), mitochondrial cytochrome c oxidase subunits I and II (*MT-CO1* and *MT-CO2* respectively code for proteins in Complex IV), ATP synthase F0 subunit 6 and ATP synthase F1 subunit alpha (*MT-ATP6* and *ATP5A*), all showed reduced transcription in SMA iHeps, but this was not correlated to severity of SMA phenotype (**Fig. 6A**). Lipid transport-related genes *ALB* and *APOA1* showed reduced transcription, whereas *APOE* showed no change in SMA iHeps (**Fig. 6B**). Lipid and cholesterol metabolism

genes acyl-CoA thioesterase 1 (*ACOT1*) and 3-hydroxy-3-methylglutaryl-CoA synthase 1 (*HMGCS1*) showed reduced transcription whereas stearoyl-CoA desaturase (*SCD1*), the rate limiting enzyme that catalyses biosynthesis of monounsaturated fatty acids that serve as substrates for de novo lipogenesis [44], had increased transcription, while sterol regulatory element binding transcription factor 1 (*SREBP1*), which plays a key role in inducing lipogenesis in the liver, showed no change (**Fig. 6C**). Fatty acid beta-oxidation (FAO)-related genes carnitine palmitoyltransferase 1A (*CPT1A*)*,* carnitine palmitoyltransferase 2 (*CPT2*), acyl-CoA synthetase long chain family member 1 (*ACSL1*), acyl-CoA dehydrogenase medium chain (*ACAD1*), and hydroxyacyl-CoA dehydrogenase trifunctional multienzyme complex subunit alpha (*HADHA*) [44] showed reduced transcription (**Fig. 6D**).

SMA patients are prone to becoming hypoglycemic after fasting [45, 46], a finding thought to be associated with altered gluconeogenesis. In line with this, gluconeogenesis-related genes phosphoenolpyruvate carboxykinase 2 (*PCK2*) and glucose-6-phosphatase catalytic subunit 1 (*G6Pase*) showed reduced transcription (**Fig. 7A**).

Genes associated with hepatic function, including glycoprotein homeostasis (*ASGR1, ASGR2*) [47], clotting (*F2*)*,* fibrosis and complement activation (*SERPINA1*) [48] and hemolysis (*HP*) [49] also showed reduced transcription (**Fig. 7B**).

Finally, *FMO1* and *FMO3*, which encodes flavin containing dimethylaniline monooxygenase-1 and -3 respectively were analyzed, as these enzymes are the primary metabolizers of risdiplam, an approved therapeutic SMN splice-modifier. *FMO3* transcription was reduced but *FMO1* was unchanged (**Fig. 7C**).

To evaluate concordance of hepatic protein expression with gene transcription and show changes in protein levels at individual iHep cell level, expression of key proteins SDHB, MT-CO1, HADHA and SMN in iHeps was analyzed using flow cytometry (**Fig. 7D**). SDHB and MT-CO1 were specifically selected as important members of electron transport chain and HADHA due to its critical role in FAO.

Concordant with reduced gene transcription, SDHB, MT-CO1 and HADHA all showed reduced expression in SMA iHeps, which associated with reduced SMN protein expression. Concordance of gene-protein expression was also noted for ATP5A and APOA1, key proteins involved in mitochondrial OXPHOS and lipid metabolism, which were hits from proteome analysis (**Fig. 4**), were downregulated in their gene transcription (**Fig. 6A** and **6B**).

These findings demonstrate that defects in SMA iHeps encompass perturbations in mRNA expression for genes involved in mitochondrial OXPHOS, lipid metabolism, gluconeogenesis, drug metabolism and hepatic function, and dysregulated expression of key proteins at single cell level. These are similar in SMA1 and SMA3.

SMA phenotype can be rescued by SMN repletion in SMA Type 1 iHeps

< Figure 8-11>

We hypothesized that primary defects in SMA liver were caused by hepatocyte SMN protein deficiency and performed CRISPR/Cas9-mediated genome editing of endogenous *SMN2* in a SMA1 iHep to study SMN-dependent effects without the confounding effect of the different genetic backgrounds of SMA patients. We converted c.840 T>C in exon 7 to engineer a *SMN1-like* gene which permanently restored functional SMN protein expression levels in the SMA1 iHep (**Supplementary Fig. S15A**) to WT levels when both *SMN2* genes were edited to create isogenic WT clones, and to 50% of WT levels when only one *SMN2* gene was edited to create isogenic carrier clones (**Supplementary Fig. S15B**).

Intracellular vacuole phenotype (**Fig. 8A)** and ORO staining (**Fig. 8B & C**) seen in SMA1 iHep and isogenic carriers, was completely rescued to WT levels by repletion of SMN protein levels and creation of isogenic WT iHeps (refer to **Fig. 1C** for WT brightfield and **Fig. 2A** for WT ORO staining images). Mean ORO staining intensity per 50 cells in each line is presented in **Supplementary Fig. S5B**. Normalisation of mean ORO staining intensity to cell number is presented in **Supplementary Fig. S5D**. Intracellular ATP, MTT, MMP and mROS levels were also rescued to near WT levels (**Fig. 9A-E**). Transcription of genes related to mitochondrial OXPHOS (**Fig. 10A**), lipid transport (**Fig. 10B**), lipid and cholesterol metabolism (**Fig. 10C**), FAO (**Fig. 10D**), gluconeogenesis (**Fig. 11A**), hepatic function (**Fig. 11B**), drug metabolism (**Fig. 11C**) and expression of key proteins in mitochondrial electron chain transport and FAO, were also rescued with repletion of SMN protein to WT levels on an isogenic background (**Fig. 11D**).

Partial rescue of SMN protein expression in isogenic carriers did not rescue steatosis in iHeps nor rescue most genes with dysregulated transcription in SMA1, suggesting that presence of only one *SMN1-like* gene cannot fully compensate for the SMA1 phenotype. This may support

a "threshold" model in which cells and tissues have differential requirements for SMN and corresponding susceptibilities to SMN depletion [14].

These specific SMN repletion and rescue findings confirm that the cellular defects described are caused by a hepatic-intrinsic deficiency in SMN.

< Figure 12>

Discussion

In this study, we provide evidence across the spectrum of SMA clinical phenotypes for susceptibility to hepatic steatosis in a SMA patient cohort and *in vitro* human models of SMA. Consistency of liver phenotype in patients and a preclinical human iPSC model provides evidence that SMN depletion predisposes SMA patients to fatty liver and liver dysfunction. Furthermore, our findings show that this is a primary liver defect resulting from hepatocyte-intrinsic SMN protein deficiency. Additionally, although the size of our patient cohort is small, the fact that steatosis was reported in a majority of patients undergoing treatment, suggests that hepato-pathology may not be adequately targeted by current therapies given at the times when these patients received treatment. Of the current therapies, onasemnogene abeparvovec and risdiplam may be expected to increase SMN levels in the liver as they act systematically. More studies are required to understand the therapeutic window for SMN-repleting therapies in extra-neuronal tissues in addition to motor neurons and how these relate to individualized therapies.

The strategy of genome editing *SMN2* to restore native SMN protein expression has been most recently used to rescue SMA phenotypes in mice [50]. Here, we used CRISPR/Cas9 genome editing to rescue SMN protein expression from endogenous *SMN2* on an isogenic background, and showed that SMN protein repletion is sufficient to rescue this hepatocyte-intrinsic SMA phenotype. To our knowledge, this is the first time such findings have been reported in SMA.

Overall, we provided new insights into the mechanisms that are responsible for fatty liver and liver dysfunction in SMA patients, and generated a hypothetical model to link these. Here, downregulation of genes and proteins relating to mitochondrial complexes II, IV and V and enzymes related to FAO, lipid synthesis and cholesterol synthesis drive abnormal lipid accumulation in SMA liver (**Fig. 12**). Although mRNA-protein expression discrepancy was noted for HMGCS1, this may be attributed to additional levels of regulation existing between transcript and protein as golgi/ER transport and protein synthesis pathways were affected (**Fig.**

3C and D). We postulated that extent of lipid accumulation identified in SMA iHeps would have functional consequences. Indeed, there are alterations in gene transcription regulating additional hepatic functions relating to: serum glycoprotein homeostasis, coagulation, complement, hemolysis, gluconeogenesis and drug metabolism. These findings are similar across various SMA genotypes. Previous studies in motor neurons and skeletal muscle have shown mitochondrial dysfunction [51] and altered ER to Golgi transport [52, 53] in SMA. Concordant with protein hits identified in our proteome analysis, proteins involved in mitochondrial oxidative phosphorylation pathway (**Fig. 3B**), ATP synthase peripheral stalk-membrane subunit b (ATP5F1), ATP synthase F1 subunit alpha (ATP5A), ATPase H+ transporting V1 subunit A (ATP6V1A) and cytochrome c1 (CYC1) were found to be dysregulated in SMN-/- mouse hippocampal neuronal cells [54] and motor neurons in a mouse model of SMA [55]. These findings of similar alterations validate our model's ability to capture elements of SMA patients' conditions and support a multi-systemic view of alterations in cellular processes in SMA.

Although most SMA patients are normally reported to be clinically asymptomatic in liver function, this may reflect the fact that liver function is not routinely checked in SMA patients, and if symptoms relating to liver dysfunction are reported by patients, they are not usually connected as related to the SMA phenotype. Furthermore, extra-neuronal organs, such as liver, are mitotic and have a tremendous capacity to regenerate and cope with disease, unlike the central nervous system, which frequently masks underlying pathology. While ultrasonic evidence of liver steatosis was present in a number of our SMA patients, this phenotype was present on histology in all SMA hiPSC-derived iHeps. This suggests that histological examination may be more sensitive than ultrasonography in detecting liver abnormalities in patients. SMN deficiency may predispose hepatocytes to functional impairment at a cellular level and increase susceptibility to multiple injuries induced by age and environmental stresses. This would be particularly relevant for the newly aging demographics of treated SMA patients [10, 13], and have implications for adverse drug reactions involving the liver such as with gene therapy. Furthermore, these data add to accumulating evidence demonstrating cell-intrinsic defects in response to SMN depletion, including muscle [56], pancreas [57], Schwann [58, 59] and endothelial cells [60].

Drugs metabolized by the liver, such as risdiplam, may not reach optimal pharmacokinetics or may cause more significant hepatotoxicity or other side-effects if their primary metabolizing

enzymes are affected. We have shown that *FMO3* transcription is SMN-dependent and reduced in SMA iHeps. FMO3 is the main metabolizer of risdiplam and makes up 75% of its metabolism [61]. Risdiplam is a lifelong treatment and if the drug induces its own metabolism by increasing SMN protein expression, risdiplam dosage may have to be increased with longer duration of treatment to maintain clinical efficacy as children with SMA age and grow. If there is already subclinical liver damage in SMA, drugs known to cause mild hepatotoxicity may cause precipitous liver failure, with severe clinical consequences including mortality. Gene therapy is known to cause mild hepatotoxicity which resolves with steroid treatment [10]. However, subacute liver failure has been reported in two children with Type 1 SMA following gene therapy, with elevations in AST, ALT, GGT and INR consistent with hepatocellular damage and defects in hepatic synthetic function, despite receiving steroids before and after infusion as per current standard of care [62]. More concerning has been the death of two children from acute liver failure in 2022 after receiving gene therapy. This has led to guidelines [63] for comprehensive pretreatment screening for liver disease in candidate SMA patients considering gene therapy [62]. Up to now, there has typically been only perfunctory examination of liver function and imaging in SMA clinics. Future studies could look into liver phenotypes of patients with severe adverse reactions to gene therapy, or patients who are non-responders to risdiplam treatment, to allow early identification of vulnerable patients so appropriate clinical management plans can be made.

Interestingly, while extra-neuronal pathology of SMA may be asymptomatic and not well-understood, there is evidence to suggest that it may have an important role in survival of motor neurons. Rescue of SMN solely in peripheral tissues, including liver, in mouse models of SMA, markedly prolongs overall survival, improves motor neuron survival and increases preservation of neuromuscular junctions [64-66]. Conversely, selective depletion of SMN in motor neurons alone results in a milder SMA phenotype as compared to systemic depletion [67], while selective restoration of SMN in neural tissue leads to only partial rescue of the SMA phenotype [68]. It is possible that effects on SMA neuromuscular function could be mediated through peripheral organ secretion of neurotrophic factors such as IGF-1, which, together with its binding protein IGFALS, has reduced expression in patients and mouse models of SMA [64, 69]. Further studies to investigate whether non-motor neuron cell autonomous SMN rescue, in liver and other peripheral organs, has a role in motor neuron function and overall survival in SMA patients, would increase our understanding of the pathology and natural history of SMA, and clinical implications of extra-neuronal and treatment modified phenotypes.

A limitation of our observational clinical study was the retrospective design and small patient numbers. However, we have provided proof of concept that ultrasonic evidence of fatty liver can be determined in SMA patients, which will enable the design of future prospective clinical studies using ultrasound to investigate prevalence of fatty liver in SMA. Liver ultrasonography is a non-invasive method of liver screening compared to liver biopsy. As a potential clinical biomarker for liver dysfunction in SMA, liver ultrasound is less painful and less expensive compared to liver biopsy, possibly more sensitive than clinically available serum markers of liver function, and widely available. Future studies may include combining imaging with expanded blood testing to discover new biomarkers associated with SMA disease processes. This will be of interest if combined with longitudinal patient follow-up for identifying patients with increased risk of adverse drug effects. Another limitation is that mitochondrial size and morphology could have confounded our analysis of MMP and mitochondrial ROS levels [73]. However, we have controlled for this using confocal microscopy (**Supplementary Fig. S14A - E**). Together with defective mitochondrial bioenergetics observed in SMA iHeps, increased mitochondrial oxidative stress level and reduced mitochondrial membrane potential suggest impaired function of mitochondria in SMA hepatocytes.

Further studies should attempt to dissect underlying molecular mechanisms and correlate these with clinical phenotypes, delineate the therapeutic window of opportunity in patients, and identify new therapeutic targets. It is the opinion of a number of researchers and clinicians that SMA therapies which increase SMN protein expression must target extra-neuronal organs for optimal management of SMA [13-15, 19, 74, 75] These treatments may synergize with SMN-independent therapies by acting in combination on several molecular pathways. Myostatin inhibitors are being studied in a number of clinical trials such as TOPAZ [76], SAPPHIRE [77], RESILIENT [78] and MANATEE [79] to see if they can rescue residual muscle defects in SMA patients and maximize clinical benefit with concurrent SMN-directed treatment. Our study suggests that drugs which treat mitochondrial dysfunction or increase FAO, such as CoQ10, riboflavin, antioxidants like Vitamin C and alpha-lipoic acid, and carnitine, may also synergize with SMN repleting therapies [80].

Our work highlights the importance of understanding extra-neuronal phenotypes of SMA in human models, and details how hiPSC and genome editing technology can be used to determine if these phenotypes are cell-intrinsic and SMN-dependent. It also provides evidence that SMA should be considered and treated as a multi-cellular and multi-organ disease. Early screening

and preventive treatment of fatty liver and other extra-neuronal phenotypes is imperative to prevent future comorbidities, and international clinical consensus is vital in establishing systematic clinical surveillance programs and therapeutic strategies which incorporate extra-neuronal phenotypes of SMA.

Materials & Methods

Sex as a Biological Variant

Our study examined male and female patients, and similar findings are reported for both sexes.

Patient Data

In this small single-center retrospective cohort study conducted at Boston Children's Hospital/Harvard Medical School, a specialty international referral center for SMA, all pediatric and adult SMA patients without any past medical history of liver disease, who were seen physically in clinic from 2020-2022, and who had received hepatic sonography or fibroscan, were included (N=8). Liver enzymes and serum markers of liver synthetic function were reviewed.

Sonographic or fibroscan steatosis grade was determined by an ultrasonogapher or pediatric gastroenterologist.

Liver steatosis was graded as follows [81]:

grade I (mild): slightly increased liver brightness relative to that of the kidney with normal visualization of the diaphragm and intrahepatic vessel borders;

grade II (moderate): increased liver brightness relative to that of the kidney with slightly impaired visualization of the intrahepatic vessels and diaphragm;

grade III (severe): markedly increased liver brightness relative to that of the kidney with poor or no visualization of the intrahepatic vessel borders, diaphragm and posterior portion of the right lobe of the liver.

Stem Cell Culture and Maintenance

Wildtype (WT)/non-SMA patient-derived stem cells (BJ, H9 and GM23720) from Corning (Corning, New York, USA) were used as a control group for comparison to patient-derived SMA cell lines obtained from Prof. Lee Rubin from Harvard University [82]. Details of SMA

patient-derived human induced pluripotent stem cells (hiPSCs) used for the stem cell model are reported in **Table 2**. CRISPR editing of the 1-38G clone was performed to engineer a c.840 T>C transition in exon 7 of *SMN2* to generate *SMN1*-like gene and derive three isogenic WTs and three isogenic carrier lines (**Table 3**). Matrigel (#354277) (Corning, New York, USA) was used to coat plates (37°C for 30 minutes) prior to seeding of hiPSCs. The matrigel was diluted in ice-cold Advanced DMEM/F-12 (#12634010) (Thermo Fisher Scientific, Massachusetts, USA) as per manufacturer's instructions. iPS Brew XF (#130-104-368) (Miltenyi Biotec, North Rhine-Westphalia, Germany) was used as the stem cell culture medium for hiPSC maintenance. hiPSCs were thawed and diluted with Advanced DMEM/F-12. After centrifugation, the supernatant was discarded and the pellet was resuspended in fresh culture medium and seeded onto the pre-coated wells. Culture medium was changed on a daily basis and hiPSCs were split using ReLeSR (#05872) (Stemcell Technologies, Vancouver, Canada) every 5-6 days when hiPSCs reach 70 - 80% confluency.

CRISPR/Cas9 Genome Editing

To derive isogenic control (repletion of two *SMN1-like* gene copies) and isogenic carrier lines (repletion of one *SMN1-like* gene copy), we performed CRISPR/Cas9 genome editing in the 1-38G patient-derived hiPSC line (SMA1). The methodology for conducting the CRISPR/Cas9 genome editing involved electroporation of sgRNA into the 1-38G hiPSC, checking of editing efficiency, isolation of clonal colonies, genotyping and off-target analysis of the clones. Finally, the acquired isogenic lines from the parental 1-38G line were frozen in cryovials in -80°C overnight and subsequently transferred to liquid nitrogen for long-term storage. The detailed methodology for how the CRISPR/Cas9 genome editing was performed can be found in the **Supplementary Methods**. The primers used for amplification and sequencing are listed in **Supplementary Table S1**.

Induced Hepatocyte (iHep) Differentiation

After splitting hiPSCs into wells in preparation for iHep differentiation, they were maintained in stem cell culture medium for two days to attain approximately 60% confluency. On day 0, the cells were cultured in RPMI/B27 basal differentiation medium (#12-702F) (Lonza, Basel, Switzerland), supplemented with 100 ng/mL of Human Activin A (#130-115-013) (Miltenyi Biotec, North Rhine-Westphalia, Germany), 3 μM of CHIR99021 (#130-106-539) (Miltenyi Biotec, North Rhine-Westphalia, Germany) and 10 μM of LY 294002 (#L-7962) (LC Laboratories, Massachusetts, USA), for 48 hours. On day 3, the cells were supplemented with

16

50 ng/mL of Human Activin A in the basal differentiation medium. On days 6 and 8, the cells were supplemented with 20 ng/mL of Human BMP-4 (#130-111-168) (Miltenyi Biotec, North Rhine-Westphalia, Germany) and 10 ng/mL of Human FGF-10 (#130-127-858) (Miltenyi Biotec, North Rhine-Westphalia, Germany) in the basal differentiation medium. From day 10 onwards, the RPMI/B27 basal differentiation medium was replaced with hepatocyte culture media (#CC-3198) (Lonza, Basel, Switzerland). On days 10, 13, 15, 17, 20 and 22, the cells were supplemented with 30 ng/mL of Human Oncostatin M IS (#130-114-942) (Miltenyi Biotec, North Rhine-Westphalia, Germany) and 50 ng/mL of Human HGF (#130-103-437) (Miltenyi Biotec, North Rhine-Westphalia, Germany). On day 24, the iHeps were harvested for further processing. The schematic representation of the differentiation protocol is as depicted in **Supplementary Fig. S2.**

Urea Assay

Conditioned hepatocyte culture media from the iHeps were collected and quantified for urea concentration using the QuantiChrom^{TM} Urea Assay kit (BioAssay Systems, USA). The optical density from each sample at 430 nm was measured and recorded using the Synergy H1 Microplate Reader (BioTek, Vermont, USA).

Oil Red Assay

Oil red assay kit was obtained from Sigma-Aldrich (St. Louis, Missouri, USA). Day24, culture media were removed and cells were washed with PBS. Next, cells were fixed with 3.7% Paraformaldehyde (Sigma Aldrich, St. Louis, Missouri, USA) at 37°C for 30 minutes. Cells were washed with ultra-pure water and incubated with 60% isopropanol at 37°C for 5 minutes. Isopropanol was removed and cells were incubated with Oil Red O working solution at 37°C for 15 minutes. Next, Oil Red O was discarded, and cells were washed with ultra-pure water until no excess stain. Next, cells were incubated with sufficient volume of hematoxylin at 37°C for 1 minute. After incubation hematoxylin was discarded and cells were washed with ultra-pure water before visualizing under a brightfield microscope (Olympus, Tokyo, Japan). Oil red images were processed using ImageJ software.

Measurement of Oxygen Consumption Rate using Seahorse XFe96 Analyzer

The oxygen consumption rate (OCR) of the Day 28 iHeps were measured using an XFe96 Seahorse Biosciences Extracellular Flux Analyzer (Agilent Technologies). Day 24 iHeps were plated in collagen coated Seahorse 96-well plate at a cell density of 2.5 x 10^5 cells for each well. The cells were allowed to recover in the 96 well plate for 4 days. Prior to the measurement of OCR, the iHeps were incubated in Seahorse XF DMEM basal media (Agilent Technologies) supplemented with 25mM of glucose (Sigma) and 1mM of Sodium Pyruvate (Gibco). The respiration profile of the iHeps were subsequently measured by the sequential injection of the following compounds: 2 μM oligomycin, 1 μM FCCP, and 1 μM rotenone/Antimycin A. Each compound treatment lasted 18 min with OCR measurements taken every 6 min. Upon completion of the seahorse assay, the iHeps cultures were immediately fixed with 4% paraformaldehyde. The iHeps cultures were stained with Hoescht 33342 (ThermoFisher) followed by imaging by high content imaging (Perkin Elmer). The final OCR values were subsequently normalized by cell count obtained to ensure consistency across OCR measurements.

MTT Assay

iHeps were trypsinized with Trypsin-EDTA (Biowest, Nuaillé, France) and Trypan Blue Assay was performed to seed 10,000 cells per well in 96-well plates. MTT assay was performed after 24 hours. 12 mM 3-(4,5-dimethylthiazol-2-yl)-2,5-diphenyl-tetrazolium bromide (MTT) (#M2003) (Sigma-Aldrich, Missouri, USA) was prepared with PBS. Spent media from 96-well plates were removed and 90 uL of fresh hepatocyte culture media was added per well. 10 uL of 12 mM MTT was added and iHeps were incubated at 37ºC for 1 hour in the dark. After 1 hour, hepatocyte culture media and MTT were removed and 100 μl of dimethyl sulfoxide (DMSO) was added . iHeps were incubated at room temperature for 1 hour in the dark. Absorbance of each well at 595 nm was measured and recorded using Synergy H1 Microplate Reader.

ATP Assay

The Molecular Probes' ATP Determination Kit (Invitrogen[TM], Massachusetts, USA) was used. iHeps were collected via trypsinization before Trypan Blue Assay to normalize cell number . Upon centrifugation and removal of supernatant, cells were lysed and centrifuged again to collect lysate supernatant. Supernatant was utilised for ATP Assay as per the manufacturer's

instruction . ATP standards of various dilutions were prepared to obtain a standard curve. Luminescence readings of the samples were performed using the Synergy H1 Microplate Reader.

Flow Cytometry

Live cells were used to assess intracellular calcium levels, mitochondrial membrane potential and mitochondrial superoxide production. Cells were trypsinized, and cell pellets were washed with PBS. Intracellular free calcium was quantified using Fluo-4 (Invitrogen^{TM}, USA). Mitochondrial membrane potential (MMP) was quantified using TMRM (Sigma Aldrich, St Louis, USA), Mitochondrial superoxide production was quantified using MitoSOX (Invitrogen^{TM}, USA).

Fixed cells were used to assess intracellular SMN (DSHB, Iowa City, USA), SDHB (Santa cruz, Texas, USA), MT-CO1 (Abcam, Cambridge, UK), HADHA (Santa cruz, Texas, USA) protein levels. Detached iHeps were incubated for 30 min with 3.7% paraformaldehyde before permeabilization for 30 min. Blocking was done with 1% BSA before 30 min incubation with SMN, SDHB, MT-CO1, HADHA antibodies.

Measurements were performed on Cytoflex LX flow cytometer (Beckman Coulter Life Sciences, Brea, California, USA) or BD LSRFortessa™ Cell Analyzer (BD Biosciences, New Jersey, USA), using 1,000,000 cells per sample. However, only 10,000 events per sample were recorded. Raw data was processed using CytoFlex software. Raw data was processed using FlowJo version 10.5.3.

Western Blot

Cells were lysed with Pierce® RIPA Lysis and Extraction buffer (Thermo Fisher Scientific, USA). Supernatant was collected after centrifugation at 13,000 g at 4°C for 20 min. Protein concentration was determined using a bicinchoninic acid (BCA) protein assay kit (Sigma Aldrich, St Louis, USA). Samples were then heated at 95°C for 5 min before being loaded and separated on precast SDS-polyacrylamide gels (Bio-Rad, Hercules, USA). Proteins were electro-transferred to a nitrocellulose membrane (Bio-Rad, Hercules, USA) in transfer buffer containing 48 mmol/l Tris-HCl, 39 mmol/l glycine, 0.037% SDS, and 20% methanol, at 4°C for 1 hour. Nonspecific binding to the membrane was blocked with 2.5% non-fat milk in TBS buffer (20 mmol/l Tris-HCl, 150 mmol/l NaCl, and 0.1% tween 20), for 1h at room temperature.

Membranes were incubated overnight (for 16 hours at least) at 4ºC with either β-actin (Sigma aldrich, St. Louis, Missouri, USA) or SMN antibody (DSHB, Iowa City, USA) in TBS buffer containing 5% BSA at the dilutions specified by the manufacturer. Binding of primary antibodies was followed by incubation with secondary horseradish peroxidase-conjugated IgG in 2.5% non-fat milk for 1h at room temperature. The blots were visualised with SuperSignal™ West Femto Maximum Sensitivity Substrate (Thermo Fisher Scientific, USA) using iBright Imaging systems (Invitrogen™). Blot images were processed using ImageJ analysis software.

RT-qPCR

TRIzol Reagent (Invitrogen™, USA) for RNA extraction was utilised as per manufacturer's instructions. cDNA was synthesized from reverse transcription of 1,000 ng of RNA (High-Capacity cDNA Reverse Transcription Kit; Applied Biosystems, USA). Reverse transcription was performed in T-Personal Thermocycler (Biometra, Germany) with conditions of 25°C for 10 min, 37°C for 120 min followed by 85°C for 5 min. RT-qPCR was carried out to quantify mRNA expression of various target genes using SYBR Green Gene Expression Assay Probes (Applied Biosystems, USA) and SYBR Green Universal PCR Master Mix (Applied Biosystems, USA). *GAPDH* was used as the housekeeping gene for both nuclear and mitochondrial encoded genes-of-interest. The RT-qPCR was performed in the 7500 Real-time PCR System (Applied Biosystems, USA) with conditions of 95°C for 10 min, followed by 95°C for 15s and 60°C for 1 min, for 40 cycles. Subsequently, the relative mRNA expression for the respective genes of interest was quantitated via the comparative CT ($\Delta\Delta$CT) method. Relevant qPCR quality controls are presented in **Supplementary Table S3.** All primer sequences can be found in **Supplementary Table S2**.

Proteomics

Cell pellets of WT and SMA iHeps were harvested on day 24, prepared appropriately and sent for tandem mass spectrometry analysis. Proteomic data from the samples were acquired using an Orbitrap Fusion Eclipse mass spectrometer (Thermo Fisher Scientific) in data-dependent mode. Detailed descriptions of sample preparation and tandem mass spectrometry analysis can be found in **Supplementary Methods**.

Statistical Analysis

For all groups, the results were presented as mean ± standard deviation (SD). Bar graphs were processed using GraphPad Prism 9.3.1 software. Comparisons involving two sample groups were performed using unpaired two-tailed Student's t-test. Comparisons involving three or more sample groups were performed using One-Way ANOVA test with Tukey's multiple comparison test. A P-value of < 0.05 is considered to be statistically significant. Outliers were assessed using ROUT test with a maximum false discovery rate (FDR) of 1%. Identified outliers were then excluded from all statistical analyses.

Study Approval

Study was approved by the Human Biomedical Research Office, Agency for Science, Technology and Research, Singapore and Boston Children's Hospital Clinical Study of Spinal Muscular Atrophy Protocol Number 05-02-028.

Data Availability

All data can be requested from the authors by correspondence. Proteomics dataset is available publicly on Japan ProteOme STandard Repository (jPOSTrepo) with the identifier YYY. Refer to "Raw Data" file for access to supporting data values.

Author contributions

Designing research studies: CJJY, BTD, WYO. Conducting experiments, acquiring data, analyzing data: DMKL, YKN, LCW, HWLK, TZ, TT, GN, RMS, WYO, CJJY. Providing reagents: RMG, SYN, AKKT, LLR. Writing the manuscript: DMKL, YKN, LCW, GN, RMG, SHP, LLR, BTD, CJJY. Co-first authors DMKL and YKN contributed to conducting experiments, acquiring data, analyzing data, writing the paper; DMKL supervised YKN on performing experiments.

Acknowledgements

References

1.   Verhaart, I.E.C., et al., *Prevalence, incidence and carrier frequency of 5q-linked spinal muscular atrophy - a literature review.* Orphanet J Rare Dis, 2017. **12**(1): p. 124.

2.   Finkel, R.S., et al., *Observational study of spinal muscular atrophy type I and implications for clinical trials.* Neurology, 2014. **83**(9): p. 810-7.

3.   Kolb, S.J., et al., *Natural history of infantile-onset spinal muscular atrophy.* Ann Neurol, 2017. **82**(6): p. 883-891.

4.   Mercuri, E., et al., *Diagnosis and management of spinal muscular atrophy: Part 1: Recommendations for diagnosis, rehabilitation, orthopedic and nutritional care.* Neuromuscul Disord, 2018. **28**(2): p. 103-115.

5.   Finkel, R.S., et al., *Diagnosis and management of spinal muscular atrophy: Part 2: Pulmonary and acute care; medications, supplements and immunizations; other organ systems; and ethics.* Neuromuscul Disord, 2018. **28**(3): p. 197-207.

6.   Wijngaarde, C.A., et al., *Population-based analysis of survival in spinal muscular atrophy.* Neurology, 2020. **94**(15): p. e1634-e1644.

7.   Wirth, B., *An update of the mutation spectrum of the survival motor neuron gene (SMN1) in autosomal recessive spinal muscular atrophy (SMA).* Hum Mutat, 2000. **15**(3): p. 228-37.

8.   Lefebvre, S., et al., *Identification and characterization of a spinal muscular atrophy-determining gene.* Cell, 1995. **80**(1): p. 155-65.

9.   Blasco-Pérez, L., et al., *Beyond copy number: A new, rapid, and versatile method for sequencing the entire SMN2 gene in SMA patients.* Hum Mutat, 2021. **42**(6): p. 787-795.

10.   Finkel, R.S., et al., *Nusinersen versus Sham Control in Infantile-Onset Spinal Muscular Atrophy.* N Engl J Med, 2017. **377**(18): p. 1723-1732.

11.   Novartis-Gene-Therapies-Inc. *Zolgensma Prescribing Information 2023*. [Accessed on 4 July 2023].

12.   U.S-Food-&-Drug-Administration., *FDA Approves Oral Treatment for Spinal Muscular Atrophy*. 2020.

13.   Mendell, J.R., et al., *Single-Dose Gene-Replacement Therapy for Spinal Muscular Atrophy.* N Engl J Med, 2017. **377**(18): p. 1713-1722.

14.   Yeo, C.J.J. and B.T. Darras, *Yeo and Darras: Extraneuronal Phenotypes of Spinal Muscular Atrophy.* Ann Neurol, 2021. **89**(1): p. 24-26.

15.   Lipnick, S.L., et al., *Systemic nature of spinal muscular atrophy revealed by studying insurance claims.* PLoS One, 2019. **14**(3): p. e0213680.

16.   Yeo, C.J.J. and B.T. Darras, *Overturning the Paradigm of Spinal Muscular Atrophy as Just a Motor Neuron Disease.* Pediatr Neurol, 2020. **109**: p. 12-19.

17.   Singh, R.N., et al., *Diverse role of survival motor neuron protein.* Biochim Biophys Acta Gene Regul Mech, 2017. **1860**(3): p. 299-315.

18.   Nash, L.A., et al., *Spinal Muscular Atrophy: More than a Disease of Motor Neurons?* Curr Mol Med, 2016. **16**(9): p. 779-792.

19.   Hamilton, G. and T.H. Gillingwater, *Spinal muscular atrophy: going beyond the motor neuron.* Trends Mol Med, 2013. **19**(1): p. 40-50.

20.   Zhang, Z., et al., *SMN deficiency causes tissue-specific perturbations in the repertoire of snRNAs and widespread defects in splicing.* Cell, 2008. **133**(4): p. 585-600.

21. Singh, R.N. and N.N. Singh, *Mechanism of Splicing Regulation of Spinal Muscular Atrophy Genes.* Adv Neurobiol, 2018. **20**: p. 31-61.

22. Lauria, F., et al., *SMN-primed ribosomes modulate the translation of transcripts related to spinal muscular atrophy.* Nat Cell Biol, 2020. **22**(10): p. 1239-1251.

23. Trefts, E., M. Gannon, and D.H. Wasserman, *The liver.* Curr Biol, 2017. **27**(21): p. R1147-r1151.

24. FDAnews. *Two Children Died After Zolgensma Gene Therapy*. 2022 [Accessed on 4 July 2023]; Available from: https://www.fdanews.com/articles/209037-two-children-died-after-zolgensma-gene-therapy.

25. Ratni, H., et al., *Discovery of Risdiplam, a Selective Survival of Motor Neuron-2 (SMN2) Gene Splicing Modifier for the Treatment of Spinal Muscular Atrophy (SMA).* J Med Chem, 2018. **61**(15): p. 6501-6517.

26. Doktor, T.K., et al., *RNA-sequencing of a mouse-model of spinal muscular atrophy reveals tissue-wide changes in splicing of U12-dependent introns.* Nucleic Acids Res, 2017. **45**(1): p. 395-416.

27. Vitte, J.M., et al., *Deletion of murine Smn exon 7 directed to liver leads to severe defect of liver development associated with iron overload.* Am J Pathol, 2004. **165**(5): p. 1731-41.

28. Szunyogova, E., et al., *Survival Motor Neuron (SMN) protein is required for normal mouse liver development.* Sci Rep, 2016. **6**: p. 34635.

29. Sahashi, K., et al., *Pathological impact of SMN2 mis-splicing in adult SMA mice.* EMBO Mol Med, 2013. **5**(10): p. 1586-601.

30. Deguise, M.O., et al., *Abnormal fatty acid metabolism is a core component of spinal muscular atrophy.* Ann Clin Transl Neurol, 2019. **6**(8): p. 1519-1532.

31. Deguise, M.O., et al., *SMN Depleted Mice Offer a Robust and Rapid Onset Model of Nonalcoholic Fatty Liver Disease.* Cell Mol Gastroenterol Hepatol, 2021. **12**(1): p. 354-377.e3.

32. Tan, L.S., et al., *Protocol for the generation of pancreatic and hepatic progenitors from human pluripotent stem cells for gene regulatory assays.* STAR Protoc, 2021. **2**(2): p. 100471.

33. Hannan, N.R., et al., *Production of hepatocyte-like cells from human pluripotent stem cells.* Nat Protoc, 2013. **8**(2): p. 430-7.

34. Levene, A.P., et al., *Is oil red-O staining and digital image analysis the gold standard for quantifying steatosis in the liver?* Hepatology, 2010. **51**(5): p. 1859; author reply 1859-60.

35. *<zolgensma.pdf>*.

36. Nicholls, D.G., *Oxidative stress and energy crises in neuronal dysfunction.* Ann N Y Acad Sci, 2008. **1147**: p. 53-60.

37. Bagkos, G., K. Koufopoulos, and C. Piperi, *A new model for mitochondrial membrane potential production and storage.* Med Hypotheses, 2014. **83**(2): p. 175-81.

38. McGivern, J.V., et al., *Spinal muscular atrophy astrocytes exhibit abnormal calcium regulation and reduced growth factor production.* Glia, 2013. **61**(9): p. 1418-1428.

39. Khayrullina, G., et al., *SMN-deficiency disrupts SERCA2 expression and intracellular Ca(2+) signaling in cardiomyocytes from SMA mice and patient-derived iPSCs.* Skelet Muscle, 2020. **10**(1): p. 16.

40. Ruiz, R., et al., *Altered intracellular Ca2+ homeostasis in nerve terminals of severe spinal muscular atrophy mice.* J Neurosci, 2010. **30**(3): p. 849-57.

41. Kawamata, H. and G. Manfredi, *Mitochondrial dysfunction and intracellular calcium dysregulation in ALS.* Mech Ageing Dev, 2010. **131**(7-8): p. 517-26.

42. Brookes, P.S., et al., *Calcium, ATP, and ROS: a mitochondrial love-hate triangle.* Am J Physiol Cell Physiol, 2004. **287**(4): p. C817-33.

43. Strasswimmer, J., et al., *Identification of survival motor neuron as a transcriptional activator-binding protein.* Hum Mol Genet, 1999. **8**(7): p. 1219-26.

44. Houten, S.M., et al., *The Biochemistry and Physiology of Mitochondrial Fatty Acid β-Oxidation and Its Genetic Disorders.* Annu Rev Physiol, 2016. **78**: p. 23-44.

45. Bruce, A.K., et al., *Hypoglycaemia in spinal muscular atrophy.* Lancet, 1995. **346**(8975): p. 609-10.

46. Berti, B., et al., *Hypoglycaemia in patients with type 1 SMA: an underdiagnosed problem?* Arch Dis Child, 2020. **105**(7): p. 707.

47. Lee, S.M., C.A. Casey, and B.L. McVicker, *Impact of asialoglycoprotein receptor deficiency on the development of liver injury.* World J Gastroenterol, 2009. **15**(10): p. 1194-200.

48. Mkaouar, H., et al., *Serine protease inhibitors and human wellbeing interplay: new insights for old friends.* PeerJ, 2019. **7**: p. e7224.

49. Ratanasopa, K., et al., *Trapping of human hemoglobin by haptoglobin: molecular mechanisms and clinical applications.* Antioxid Redox Signal, 2013. **18**(17): p. 2364-74.

50. Arbab, M., et al., *Base editing rescue of spinal muscular atrophy in cells and in mice.* Science, 2023. **380**(6642): p. eadg6518.

51. Zilio, E., V. Piano, and B. Wirth, *Mitochondrial Dysfunction in Spinal Muscular Atrophy.* Int J Mol Sci, 2022. **23**(18).

52. Powis, R.A., et al., *Systemic restoration of UBA1 ameliorates disease in spinal muscular atrophy.* JCI Insight, 2016. **1**(11): p. e87908.
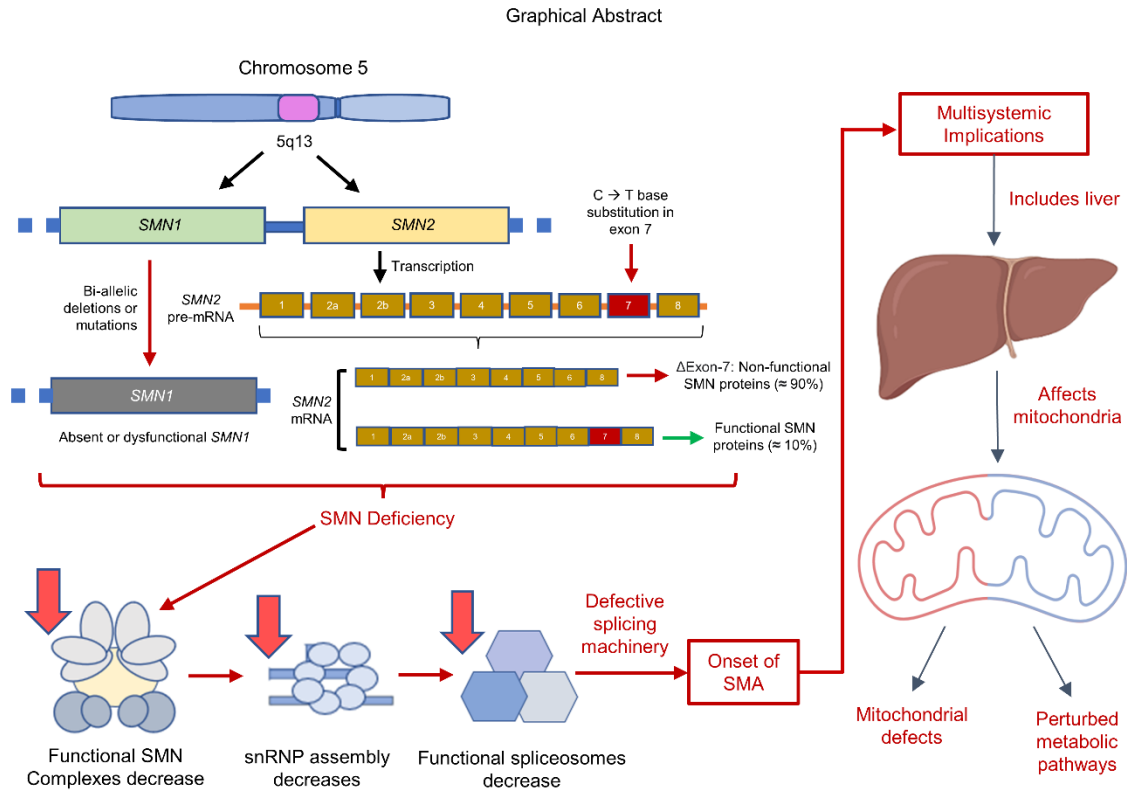
53.   Li, H., et al., *α-COP binding to the survival motor neuron protein SMN is required for neuronal process outgrowth.* Hum Mol Genet, 2015. **24**(25): p. 7295-307.

54.   Wishart, T.M., et al., *SMN deficiency disrupts brain development in a mouse model of severe spinal muscular atrophy.* Hum Mol Genet, 2010. **19**(21): p. 4216-28.

55.   Wishart, T.M., et al., *Dysregulation of ubiquitin homeostasis and β-catenin signaling promote spinal muscular atrophy.* J Clin Invest, 2014. **124**(4): p. 1821-34.

56.   Hayhurst, M., et al., *A cell-autonomous defect in skeletal muscle satellite cells expressing low levels of survival of motor neuron protein.* Dev Biol, 2012. **368**(2): p. 323-34.

57.   Bowerman, M., et al., *Glucose metabolism and pancreatic defects in spinal muscular atrophy.* Ann Neurol, 2012. **72**(2): p. 256-68.

58.   Hunter, G., et al., *SMN-dependent intrinsic defects in Schwann cells in mouse models of spinal muscular atrophy.* Hum Mol Genet, 2014. **23**(9): p. 2235-50.

59.   Hunter, G., et al., *Restoration of SMN in Schwann cells reverses myelination defects and improves neuromuscular function in spinal muscular atrophy.* Hum Mol Genet, 2016. **25**(13): p. 2853-2861.

60.   Zhou, H., et al., *Microvasculopathy in spinal muscular atrophy is driven by a reversible autonomous endothelial cell defect.* J Clin Invest, 2022. **132**(21).

61.   Cleary, Y., et al., *Estimation of FMO3 Ontogeny by Mechanistic Population Pharmacokinetic Modelling of Risdiplam and Its Impact on Drug-Drug Interactions in Children.* Clin Pharmacokinet, 2023. **62**(6): p. 891-904.

62.   Feldman, A.G., et al., *Subacute Liver Failure Following Gene Replacement Therapy for Spinal Muscular Atrophy Type 1.* J Pediatr, 2020. **225**: p. 252-258.e1.

63.   *FDA-Label-Search. FDA Online Label Repository.*   [Accessed on 4 July 2023]; Available from: labels.fda.gov/.

64. Hua, Y., et al., *Motor neuron cell-nonautonomous rescue of spinal muscular atrophy phenotypes in mild and severe transgenic mouse models.* Genes Dev, 2015. **29**(3): p. 288-97.

65. Hua, Y., et al., *Peripheral SMN restoration is essential for long-term rescue of a severe spinal muscular atrophy mouse model.* Nature, 2011. **478**(7367): p. 123-6.

66. Reilly, A., et al., *Long term peripheral AAV9-SMN gene therapy promotes survival in a mouse model of spinal muscular atrophy.* Human Molecular Genetics, 2024. **33**(6): p. 510-519.

67. Park, G.H., et al., *Reduced survival of motor neuron (SMN) protein in motor neuronal progenitors functions cell autonomously to cause spinal muscular atrophy in model mice expressing the human centromeric (SMN2) gene.* J Neurosci, 2010. **30**(36): p. 12005-19.

68. Passini, M.A., et al., *CNS-targeted gene therapy improves survival and motor function in a mouse model of spinal muscular atrophy.* J Clin Invest, 2010. **120**(4): p. 1253-64.

69. Kaymaz, A.Y., et al., *Alterations in insulin-like growth factor system in spinal muscular atrophy.* Muscle Nerve, 2022. **66**(5): p. 631-638.

70. Brand, M.D. and D.G. Nicholls, *Assessing mitochondrial dysfunction in cells.* Biochem J, 2011. **435**(2): p. 297-312.

71. Chemello, F., et al., *Dysfunctional mitochondria accumulate in a skeletal muscle knockout model of Smn1, the causal gene of spinal muscular atrophy.* Cell Death Dis, 2023. **14**(2): p. 162.

72. Ando, S., et al., *Edaravone is a candidate agent for spinal muscular atrophy: In vitro analysis using a human induced pluripotent stem cells-derived disease model.* Eur J Pharmacol, 2017. **814**: p. 161-168.

73. Kowaltowski, A.J., *Strategies to detect mitochondrial oxidants.* Redox Biol, 2019. **21**: p. 101065.

74. Simone, C., et al., *Is spinal muscular atrophy a disease of the motor neurons only: pathogenesis and therapeutic implications?* Cell Mol Life Sci, 2016. **73**(5): p. 1003-20.

75. Yeo, C.J.J., et al., *Ethical Perspectives on Treatment Options with Spinal Muscular Atrophy Patients.* Ann Neurol, 2022. **91**(3): p. 305-316.

76. Business-Wire. *Positive Phase 2 TOPAZ Trial Extension Data Demonstrate Sizable and Sustained Motor Function Improvement at 24 Months with Apitegromab for Non-Ambulatory Patients with Types 2 and 3 Spinal Muscular Atrophy (SMA).* [Accessed on 4 July 2023]; Available from: https://www.businesswire.com/news/home/20220617005087/en/Positive-Phase-2-Topaz-Trial-Extension-Data-Demonstrate-Sizable-and-Sustained-Motor-Function-Improvement-at-24-Months-with-Apitegromab-for-Non-Ambulatory-Patients-with-Types-2-and-3-Spinal-Muscular-Atrophy-SMA.

77. Spinal-Muscular-Atrophy-Support-UK. *Sapphire Trial Results and Updates* [Accessed on 4 July 2023]; Available from: https://smauk.org.uk/treatments-research/drugs-being-tested-clinical-trials/apitegromab-scholar-rock/sapphire-trial-results/.

78. SMAtrial.com. *About the Investigational Medication. What is Taldefgrobep alfa?* . [Accessed on 4 July 2023]; Available from: https://www.smatrial.com/investigational-medication.

79. SMA-Foundation. *Roche shares an update on MANATEE clinical study*. 2021 [Accessed on 4 July 2023]; Available from: https://smafoundation.org/sma-press/roche-shares-an-update-on-manatee-clinical-study/.

80. El-Hattab, A.W., et al., *Therapies for mitochondrial diseases and current clinical trials.* Mol Genet Metab, 2017. **122**(3): p. 1-9.

81.   Gerstenmaier, J.F. and R.N. Gibson, *Ultrasound in chronic liver disease.* Insights Imaging, 2014. **5**(4): p. 441-55.

82.   Rodriguez-Muela, N., et al., *Single-Cell Analysis of SMN Reveals Its Broader Role in Neuromuscular Disease.* Cell Rep, 2017. **18**(6): p. 1484-1498.

83.   Lala, V., M. Zubair, and D.A. Minter, *Liver Function Tests*, in *StatPearls*. 2023, StatPearls Publishing

Graphical Abstract

Graphical Abstract

Graphical abstract. Portions of the figures created with BioRender.com.
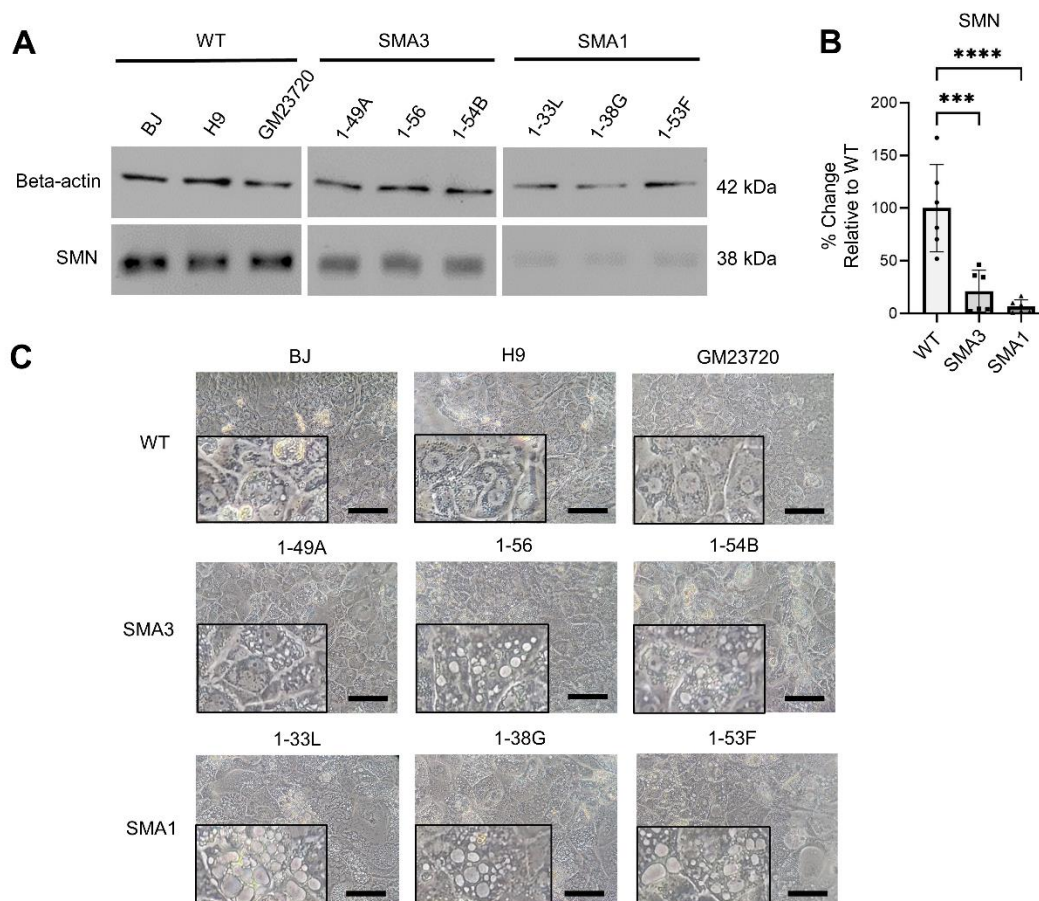
Figure 1

Figure 1. Day 24 SMA iHeps showed larger vacuoles. (A) Protein quantification of SMN expression between Day 24 WT and SMA iHeps by western blot with beta-actin as the housekeeping protein for normalisation, **(B)** with ImageJ analysis. Data is from two independent experiments, each with three biological replicates (WT n=6, SMA1 n=6, SMA3 n=6). **(C)** Brightfield microscope images of Day 24 WT and SMA iHeps. Scale bar = 50 μm. Boxed portions represent zoomed-in segments of the original image to showcase vacuole enlargement more clearly. **(B)** Data were analyzed using One-Way ANOVA test with Tukey's multiple comparison test. Data are presented as mean ($\pm$SD). * p-value < 0.05; ** p-value < 0.01; *** p-value < 0.001; **** p-value < 0.0001.
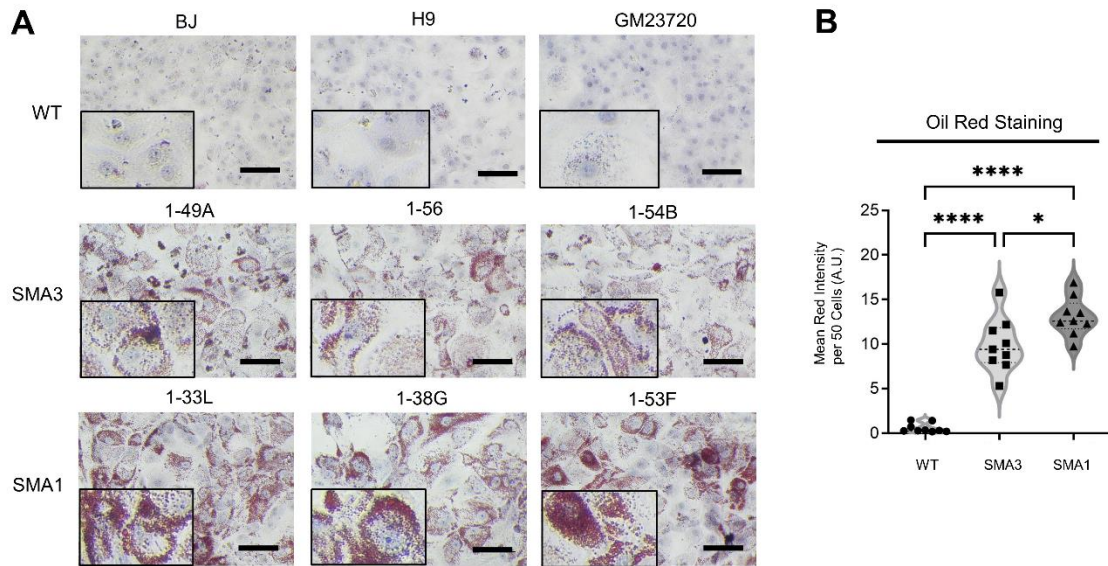
Figure 2

Figure 2. Day 24 SMA iHeps showed increased lipid accumulation. (A) Oil red staining of Day 24 WT and SMA iHeps (scale bar = 50 μm) and **(B)** ImageJ analysis. Haematoxylin stains nuclear components and Oil red O stains neutral triglycerides and lipids. Boxed portions represent zoomed-in segments of the original image to showcase oil red staining of triglycerides and lipids with more clarity. **(B)** The mean red intensity of 50 cells is presented. Data is representative of three independent experiments, each with three biological replicates (WT n=9, SMA1 n=9, SMA3 n=9). Data were analyzed using One-Way ANOVA test with Tukey's multiple comparison test. Data are presented as mean (±SD). * p-value < 0.05; ** p-value < 0.01; *** p-value < 0.001; **** p-value < 0.0001.
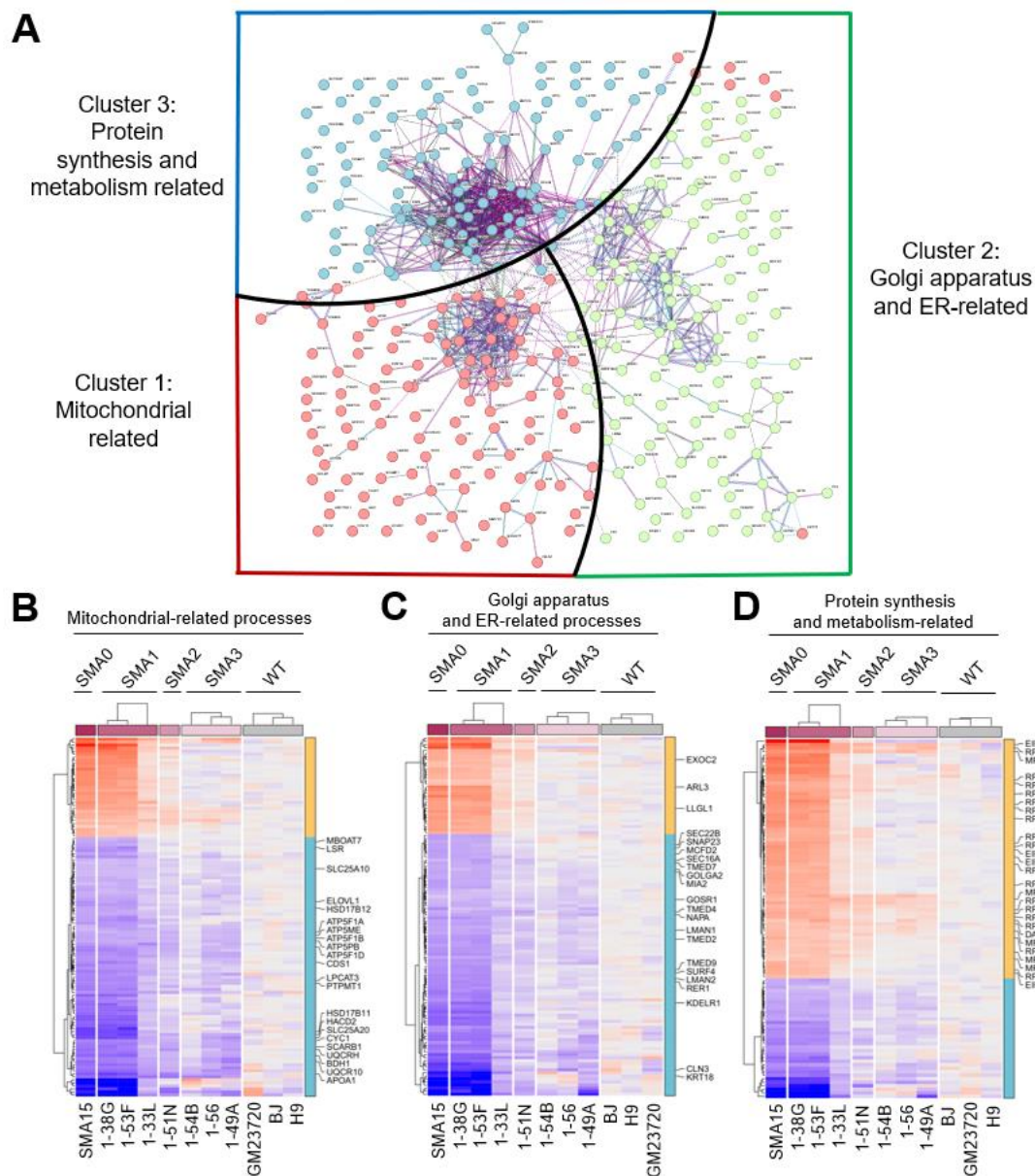
Figure 3

Figure 3. Proteomics analysis of Day 24 WT and SMA iHeps. (A) 343 proteins that showed significant differences in SMA patient-derived iHeps cell lines compared to wild-type patient cell lines were analysed for their interactions on the STRING database. Proteins in individual clusters were subjected to term enrichment analysis using the ShinyGO app. Cluster 1 (red), Cluster 2 (green) and Cluster 3 (blue) suggested that there were mitochondria-related processes, enrichment of golgi apparatus and endoplasmic reticulum related processes, and enrichment of protein synthesis and metabolism related processes in the interaction network using the UniProt database. **(B-D)** Heatmap demonstration of significantly regulated proteins between SMA and WT iHeps, with proteins implicated in oxidative phosphorylation and lipid metabolism (cluster 1), golgi vesicle transport (cluster 2) and protein translation (cluster 3) highlighted.

Figure 4

Figure 4. Proteins implicated in mitochondrial processes and lipid metabolism. Protein hits for **(A)** mitochondria and **(B)** lipid metabolism processes based on the UniProt database were used to generate heatmap. **(C)** Differentially expressed proteins between WT, SMA3, SMA2, SMA1 and SMA0 derived iHeps involved in fatty acid oxidation, lipid transport, triglyceride accumulation, and cholesterol metabolism respectively.
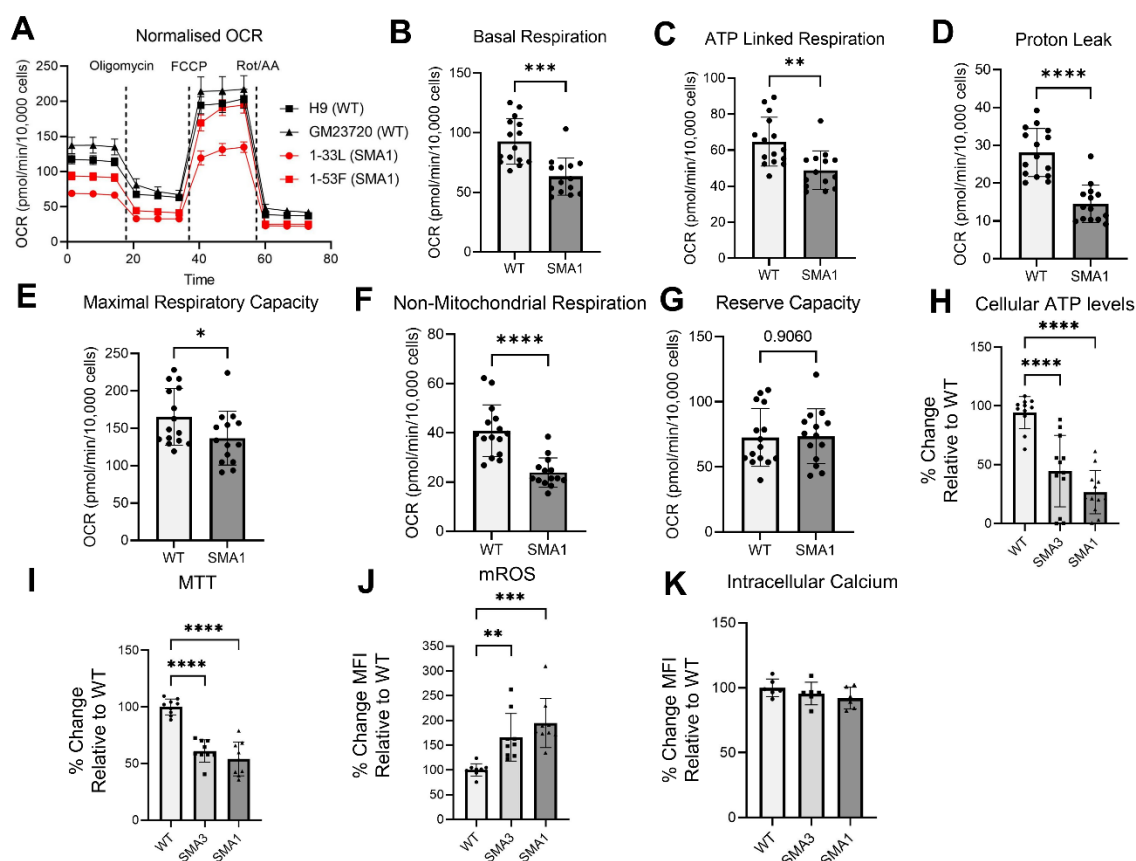
Figure 5.

Figure 5. Functional assays showing metabolic dysfunction in Day 24 SMA iHeps. (A) Measurements of oxygen consumption rate (OCR) between WT and SMA Type 1 (SMA1) iHeps (error bars=SEM, H9 n=8, GM23720 n=7, 1-33L n=6, 1-53F n=8, H9 and GM23720 are biological replicates for WT, 1-33L and 1-53F are biological replicates for SMA1), with analysis of **(B)** Basal respiration, **(C)** ATP linked respiration, **(D)** proton leak, **(E)** maximal respiratory capacity, **(F)** non-mitochondrial respiration and **(G)** mitochondrial reserve capacity. **B – G:** (WT n= 15, SMA1 n=14). Cellular assays in D24 iHeps measuring **(H)** intracellular ATP (WT n=11, SMA1 n=12, SMA3 n=12, each with three biological replicates). One outlier from WT was removed using the ROUT test with a maximum false discovery rate (FDR) of 1%. Data is from four independent experiments. **(I)** Cellular metabolic activity by MTT assay. **(J)** Mitochondrial ROS levels by MitoSOX assay. **I – J**: WT n=9, SMA1 n=9, SMA3 n=9, each with three biological replicates, data is from three independent experiments. **(K)** Intracellular cytosolic calcium levels by Fluo-4 AM assay (WT n=6, SMA1 n=6, SMA3 n=6, each with three biological replicates, data is from two independent experiments). **J – K:** Flow cytometry was performed to obtain MFI, where 10,000 events were recorded and viable cells were then gated. **B – G:** Data was analyzed by unpaired student's t-test. **H – K:** Data were

analyzed using One-Way ANOVA test with Tukey's multiple comparison test. Data are presented as mean (±SD). * p-value < 0.05; ** p-value < 0.01; *** p-value < 0.001; **** p-value < 0.0001.
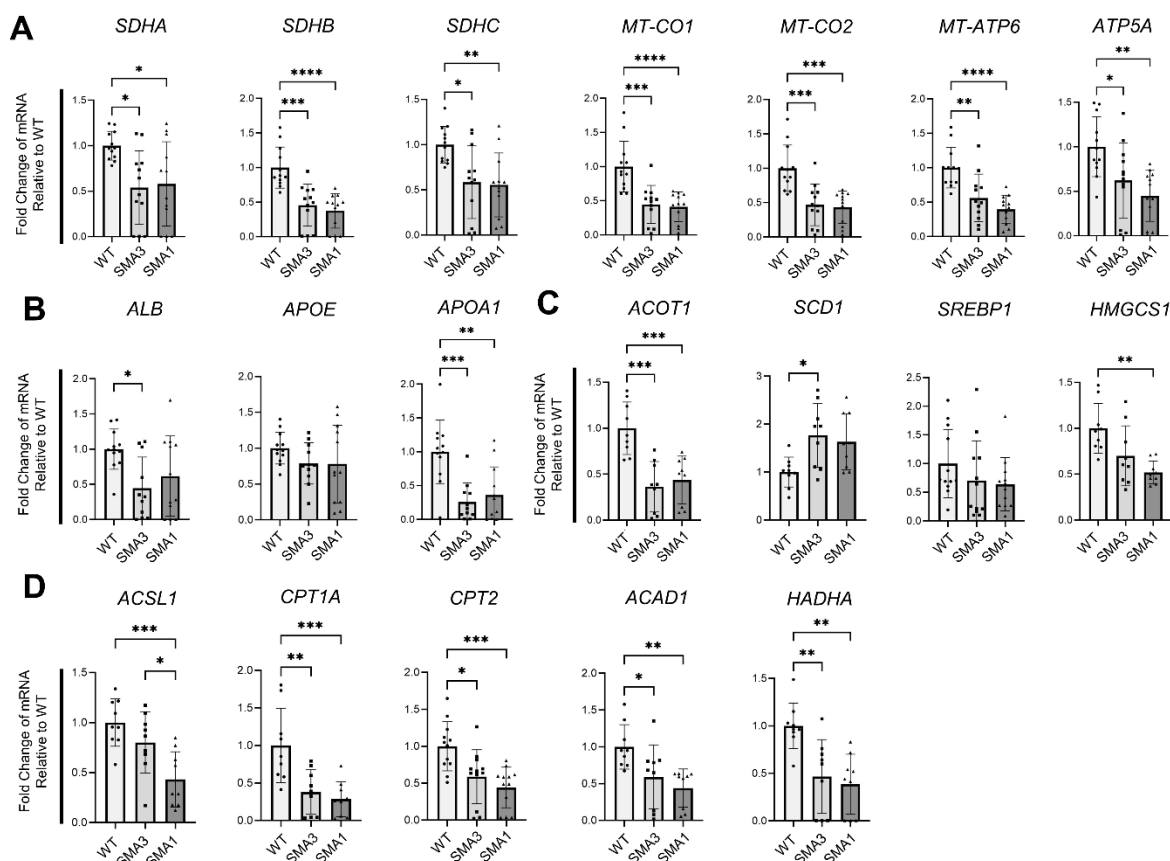
Figure 6

Figure 6. Day 24 SMA iHeps show dysregulation of genes implicated in mitochondrial function and lipid metabolism. (A) RT-qPCR of mitochondrial OXPHOS-related genes. **(B)** RT-qPCR of lipid transport genes. For *ALB*, *APOE*, and *APOA1*, one outlier from SMA3 was removed using the ROUT test with a maximum false discovery rate (FDR) of 1%. **(C)** RT-qPCR of lipid and cholesterol synthesis pathway genes. **(D)** RT-qPCR of beta-oxidation pathway genes. Data is from three to four independent experiments, each with three biological replicates. **(A – D)** Unless specifically indicated that outliers were removed, analysis of data from three independent experiments included nine samples (n=9) each for WT, SMA3 and SMA1 conditions. Similarly for analysis of data from four independent experiments, n=12 for each condition. Data were analyzed using One-Way ANOVA test with Tukey's multiple comparison test. Data are presented as mean (±SD). * p-value < 0.05; ** p-value < 0.01; *** p-value < 0.001; **** p-value < 0.0001.
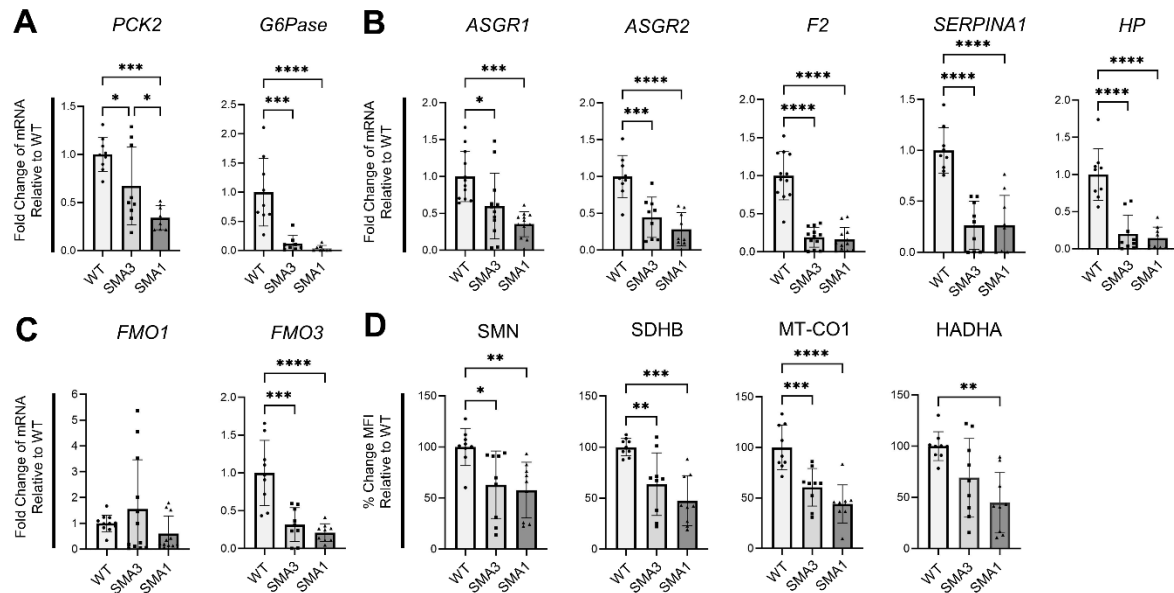
Figure 7

Figure 7. Day 24 SMA iHeps show dysregulation of genes implicated in gluconeogenesis and drug metabolism genes and critical proteins involved in mitochondrial electron transport chain and fatty acid oxidation. (A) RT-qPCR of gluconeogenesis pathway genes. For *PCK2*, one outlier from SMA1 was removed using the ROUT test with a maximum false discovery rate (FDR) of 1%. For *G6Pase*, one outlier from SMA3 and SMA1 was removed. **(B)** RT-qPCR of iHep function genes. **(C)** RT-qPCR of drug metabolism genes. For *FMO1*, one outlier from SMA1 was removed. **(A - C)** For all RT-qPCR, fold change results were derived using the comparative $\Delta\Delta$Ct method. **(D)** Flow cytometry analysis of critical proteins involved in mitochondrial electron transport chain, SDHB and MT-CO1, and fatty acid oxidation, HADHA, with correlation to SMN protein expression in Day 24 SMA iHeps. MFI readings were obtained through the recording of 10,000 events followed by gating of the viable iHeps. **(A - D)** Unless specifically indicated that outliers were removed, analysis of data from three independent experiments included nine samples (n=9) each for WT, SMA3 and SMA1 conditions. Similarly for analysis of data from four independent experiments, n=12 for each condition. Data were analyzed using One-Way ANOVA test with Tukey's multiple comparison test. Data are presented as mean ($\pm$SD). * p-value < 0.05; ** p-value < 0.01; *** p-value < 0.001; **** p-value < 0.0001.
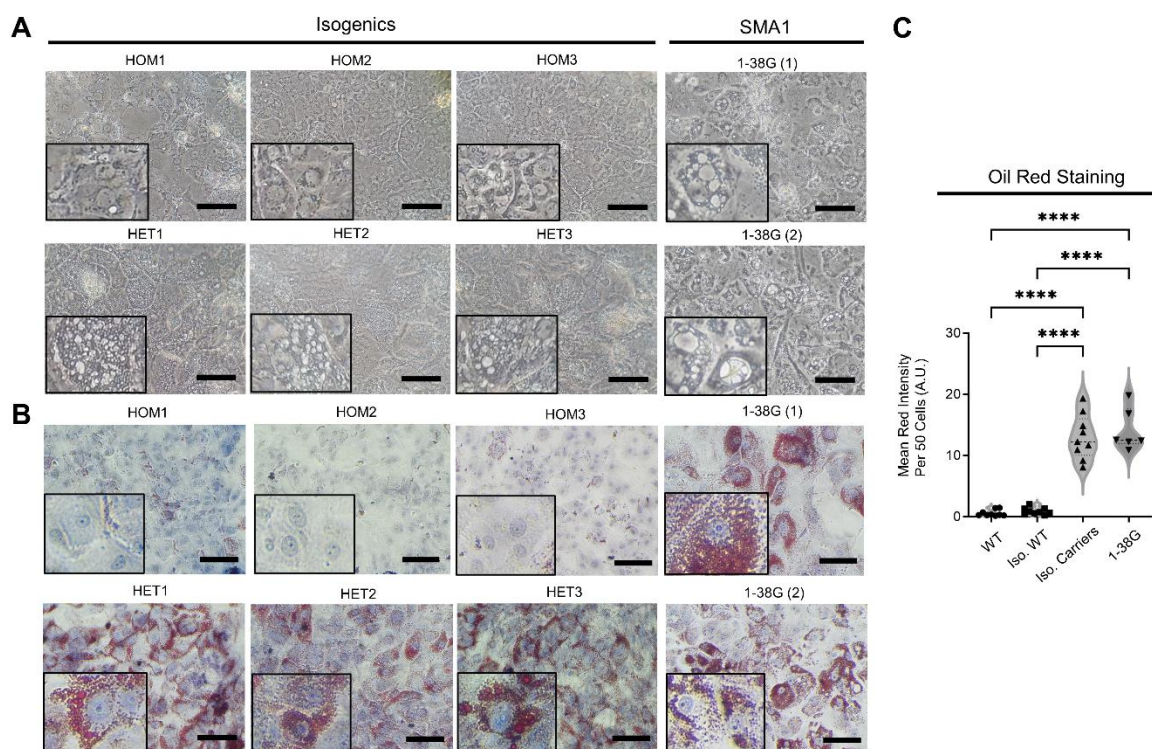
Figure 8

Figure 8. Rescue of lipid accumulation with SMN repletion in Day 24 SMA Type 1 iHeps.
(A) Brightfield microscope images of Day 24 isogenic WT, isogenic carriers and 1-38G (SMA1) iHeps. Scale bar = 50 μm. Boxed portions represent zoomed-in segments of the original image to showcase vacuole enlargement more clearly. **(B)** Oil red O (ORO) staining of Day 24 isogenic WT, isogenic carriers and 1-38G iHeps, showing decrease in lipid accumulation after repletion of SMN. Scale bar = 50 μm. Boxed portions represent zoomed-in segments of the original image to showcase oil red staining of triglycerides and lipids with more clarity. **(C)** The mean red intensity of 50 cells is presented. WT, Iso. WT and Iso. Carriers has 3 biological replicates. Data is representative of three independent experiments (WT n=9, Iso. WT n=9, Iso. Carriers n=9, 1-38G n=6). Data were analyzed using One-Way ANOVA test with Tukey's multiple comparison test. Data are presented as mean (±SD). * p-value < 0.05; ** p-value < 0.01; *** p-value < 0.001; **** p-value < 0.0001.

Figure 9

Figure 9. Rescue of metabolic dysfunction with SMN repletion in Day 24 SMA Type 1 iHeps. Cellular assays in d24 iHeps measuring **(A)** intracellular ATP (WT n=9, Iso. WT n=9, Iso. Carriers n=9, 1-38G n=4)**(B)** Cellular metabolic activity by MTT assay (WT n=9, Iso. WT n=9, Iso. Carriers n=9, 1-38G n=4) **(C)** mitochondrial membrane potential (MMP) by TMRM assay (WT n=9, Iso. WT n=9, Iso. Carriers n=9, 1-38G n=6). **(D)** mitochondrial ROS levels by MitoSOX assay (WT n=9, Iso. WT n=9, Iso. Carriers n=9, 1-38G n=5) **(A − D)** Data is from three independent experiments. WT, Iso. WT and Iso. Carriers has 3 biological replicates. **(E)** intracellular cytosolic calcium levels by Fluo-4 AM assay Data is from two independent experiments (WT n=6, Iso. WT n=6, Iso. Carriers n=6, 1-38G n=4) **(C − E)** MFI for TMRM, MitoSOX and Fluo-4 AM assays were obtained using flow cytometry, where 10,000 events were recorded, and the viable cells were then gated. **(A − E)** All results were quantified as a percentage relative to the mean of the WTs. Data were analyzed using One-Way ANOVA test with Tukey's multiple comparison test. Data are presented as mean (±SD). * p-value < 0.05; ** p-value < 0.01; *** p-value < 0.001; **** p-value < 0.0001.
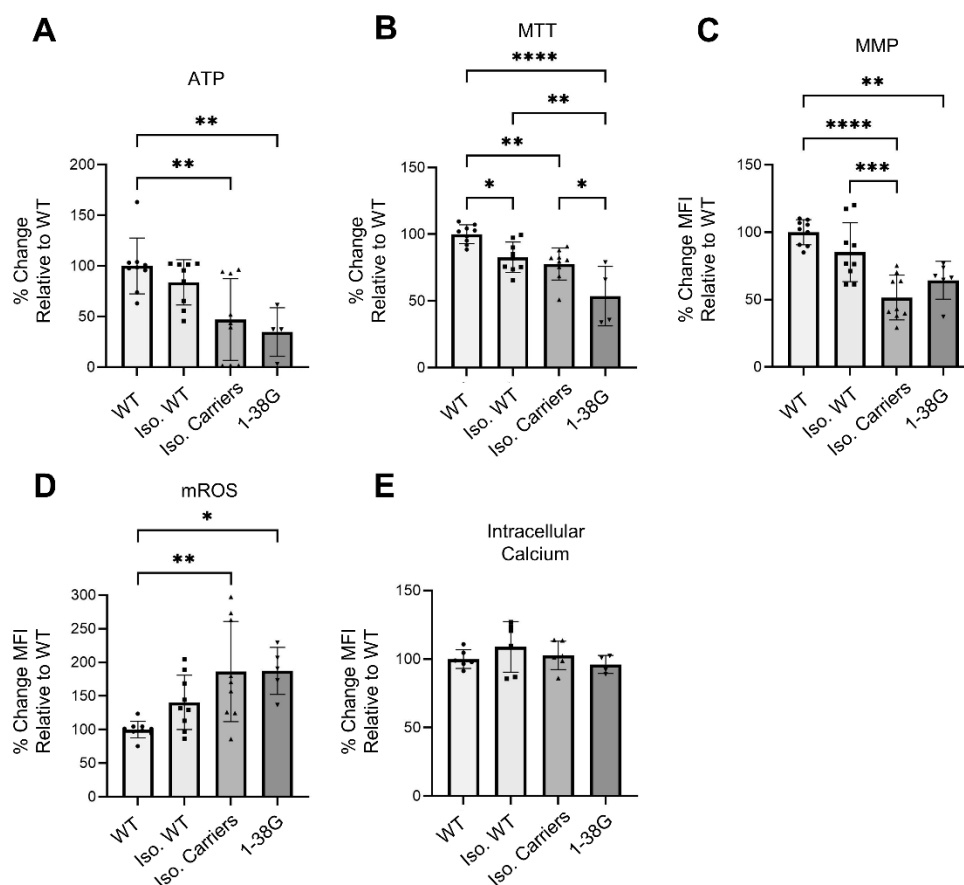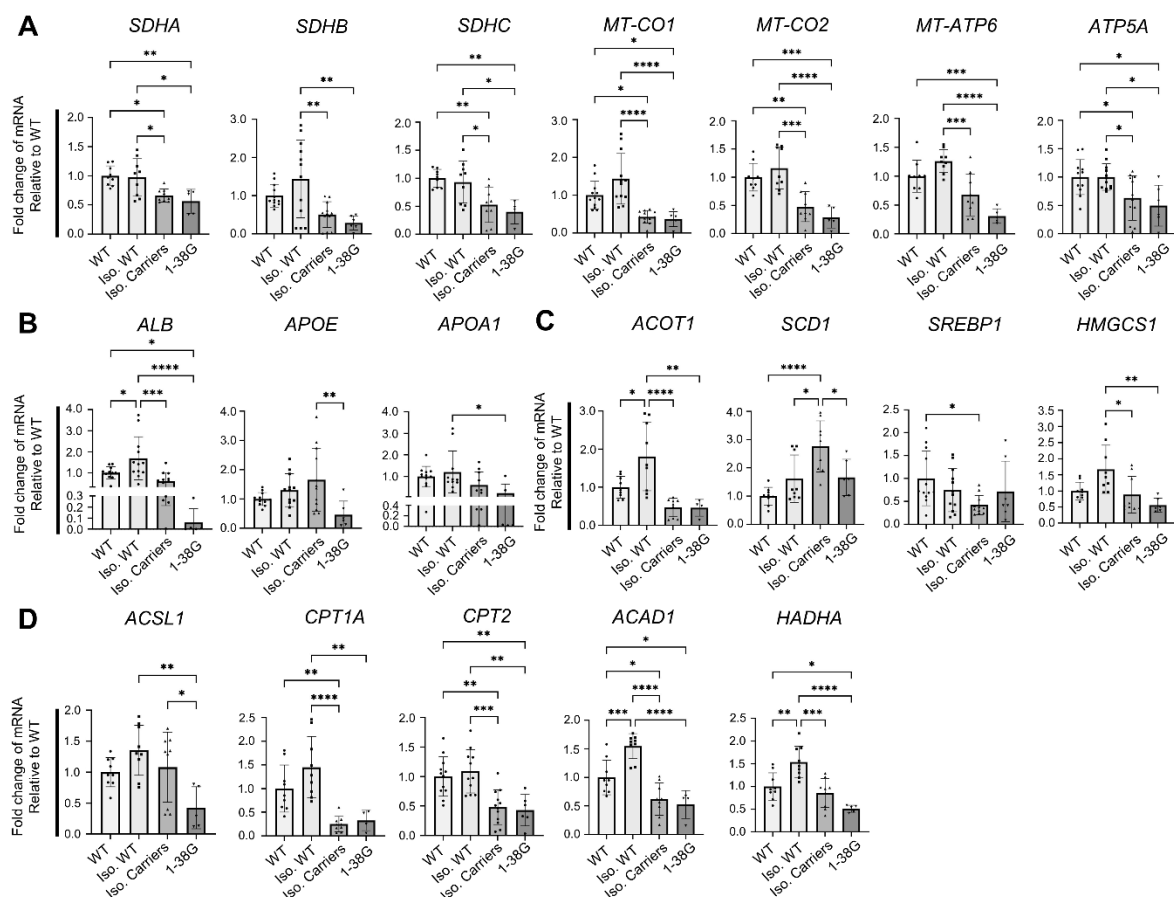
Figure 10

Figure 10. Rescue of genes implicated in mitochondrial function and lipid metabolism with SMN repletion in Day 24 SMA Type 1 iHeps. (A) RT-qPCR of mitochondrial OXPHOS-related genes. (B) RT-qPCR of lipid transport genes. For *ALB*, one outlier from 1-38G was removed using the ROUT test with a maximum false discovery rate (FDR) of 1%. For *APOA1*, two outliers from Iso. Carriers and one outlier from iso. WT was removed. (C) RT-qPCR of lipid and cholesterol synthesis pathway genes. For *SREBP1*, one outlier from Iso. Carriers was removed. (D) RT-qPCR of fatty acid beta-oxidation pathway genes. Data is from three to four independent experiments For *CPT2*, one outlier from Iso. WT was removed. (A-D) Data is from three to four independent experiments. Unless specifically indicated that outliers were removed, analysis of data from three independent experiments included nine samples (n=9) each for WT, Iso. WT, Iso. Carrier conditions. Similarly for analysis of data from four independent experiments, n=12 for each condition. For 1-38G, n≥4 for all experiments. Data were analyzed using One-Way ANOVA test with Tukey's multiple comparison test. Data are presented as mean (±SD). * p-value < 0.05; ** p-value < 0.01; *** p-value < 0.001; **** p-value < 0.0001.
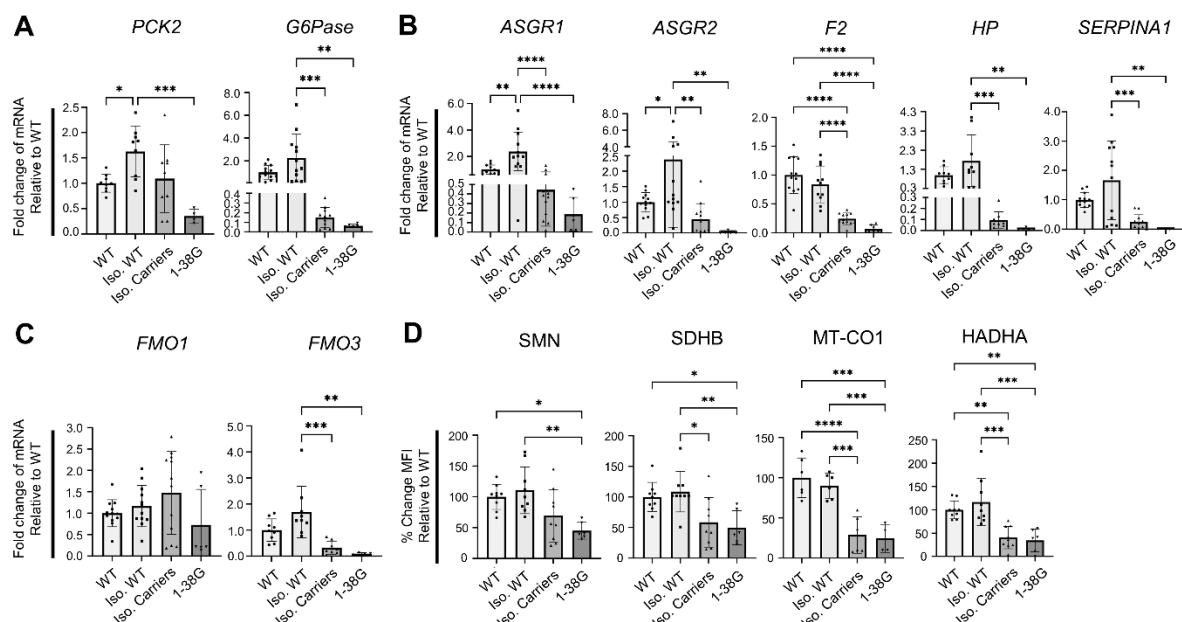
Figure 11

Figure 11. Rescue of genes implicated in gluconeogenesis and drug metabolism genes and critical proteins involved in mitochondrial electron transport chain and fatty acid oxidation with SMN repletion in Day 24 SMA Type 1 iHeps. (A) RT-qPCR of gluconeogenesis pathway genes. For *G6Pase*, one outlier from Iso. Carrier and one outlier from 1-38G was removed using the ROUT test with a maximum false discovery rate (FDR) of 1%. **(B)** RT-qPCR of iHep function genes. For *ASGR2*, one outlier from 1-38G was removed. For *F2*, one outlier from Iso. WT was removed. For *SERPINA1*, one outlier from 1-38G. **(C)** RT-qPCR of drug metabolism genes. For *FMO3*, one outlier from Iso. Carriers was removed. **(A-C)** For all RT-qPCR, fold change results were derived using the comparative ΔΔCt method. Data is from three to four independent experiments. Unless specifically indicated that outliers were removed, analysis of data from three independent experiments included nine samples (n=9) each for WT, Iso. WT, Iso. Carrier conditions. Similarly for analysis of data from four independent experiments, n=12 for each condition. For 1-38G, n≥4 for all experiments. **(D)** Flow cytometry analysis of critical proteins involved in mitochondrial electron transport chain, SDHB and MT-CO1, and fatty acid oxidation, HADHA, with correlation to SMN protein expression. MFI was obtained by recording 10,000 events and viable iHeps were then gated for. Data is from two to three independent experiments. Analysis of data from two independent experiments included nine samples (n=6) each for WT, Iso. WT, Iso. Carrier conditions. Similarly for analysis of data from three independent experiments, n=9 for each condition. For 1-38G, n≥4 for all experiments. **(A-D)** Data were analyzed using One-Way ANOVA test with

Tukey's multiple comparison test. Data are presented as mean (±SD). * p-value < 0.05; ** p-value < 0.01; *** p-value < 0.001; **** p-value < 0.0001.
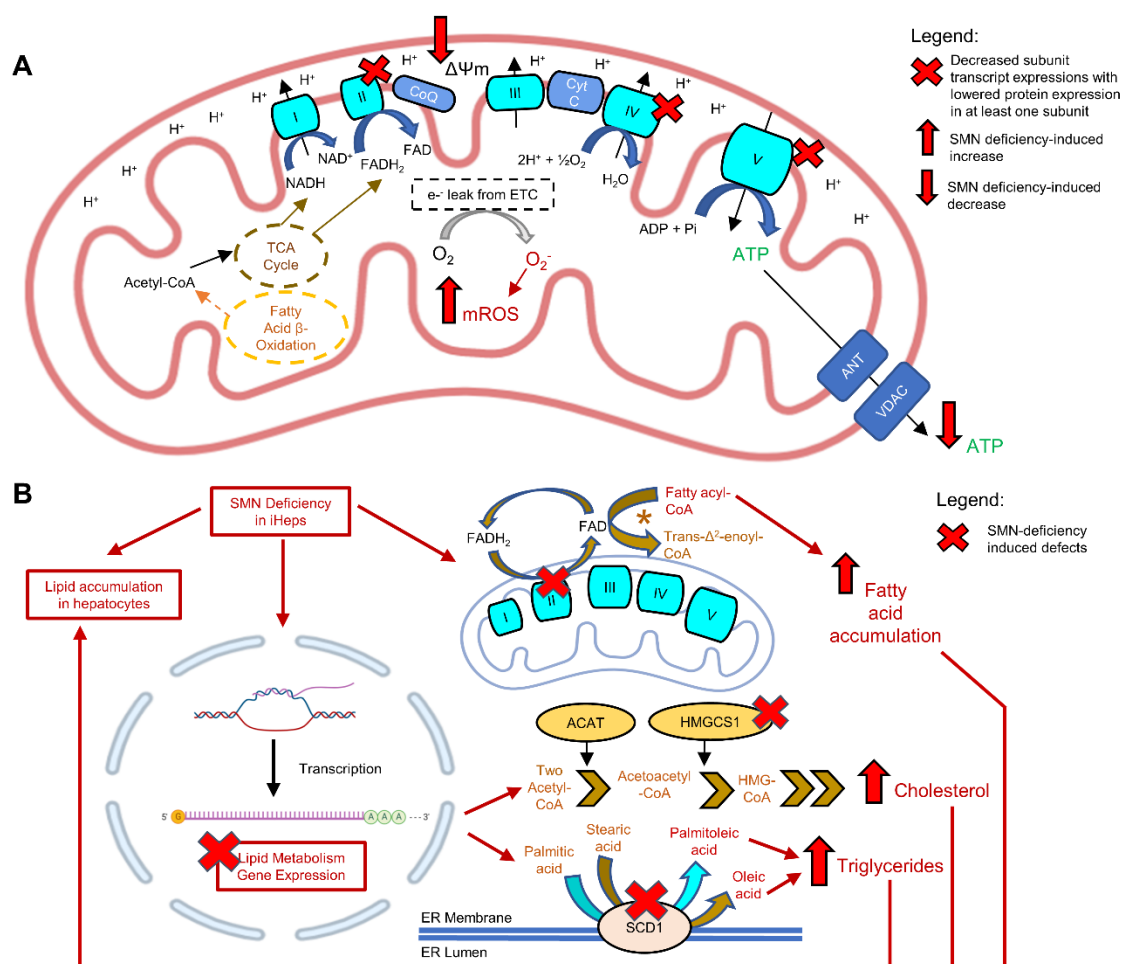
Figure 12

Figure 12. Schematic diagram of proposed mitochondrial dysfunction and lipid metabolism defects in SMA iHeps. **(A)** Mitochondrial dysfunction in SMA iHeps. Dysfunction / dysregulation in mitochondrial complexes II, IV and V, and VDAC, as a result of decreased mRNA and/or protein subunit expressions. **(B)** Lipid metabolism defects in SMA iHeps. Lipid metabolism gene expression dysregulation includes enzymes involved in fatty acid beta-oxidation, lipid synthesis and cholesterol synthesis pathways. Increased fatty acid accumulation due to cross-talk defects between mitochondria and fatty acid beta-oxidation, increased cholesterol synthesis due to increased protein expression of HMGCS1, and increased triglyceride synthesis due to increased expression of *SCD1* mRNA may account for overall lipid accumulation in SMA iHeps, as observed from Oil red staining assay. **(A - B)** Portions of the figures created with BioRender.com.

Table 1. Clinical Findings of Liver Pathology in SMA Patients.

Patient Demographics								
Age	3	5	5	7	19	52	6	24
Sex	F	F	F	M	F	F	M	M
SMA Type	1	1	1	1	2	2	2	3
Liver Imaging								
Liver Ultrasound	Yes	Yes	Yes	Yes	Yes	Yes	Yes	Yes
Liver Fibroscan	No	No	No	No	No	Yes	Yes	No
Clinical Findings								
Liver Fibrosis	No	No	No	No	No	Minimal	No	No
Fatty Liver	Yes (mild to moderate)	Yes (mild to moderate)	No	No	Yes (mild to moderate)	Yes (mild to moderate)	Yes (mild to moderate)	Yes (mild to moderate)
AST (40)[a]	25	23	31	55	41	41	25	40
ALT (30)[a]	16	15	13	40[b]	**101**[c]	43[d]	9	50
GGT (35)[a]	9	11	-	115[b]	26	**406**[d]	10	-
Albumin (46)[a]	3.9	4.8	4.1	4.2	3	3.5	4.5	7.9
Protein (8.2)[a]	7.4	7.1	6.3	7.1	6.2	6.9	7.1	5.2
Total Bilirubin (1.2)[a]	<0.2	0.2	0.2	0.2	0.2	0.3	0.2	0.5
Fasting glucose (100)	88	96	-	-	**113**[c]	-	87	-
SMA Treatment								
Spinraza	Yes	Yes	Yes	No	Yes	No	Yes	Yes
Zolgensma	Yes	No	No	No	No	No	Yes	No
Risdiplam	Yes	No	No	Yes	Yes	Yes	No	No

In this single-center retrospective cohort study, 8 pediatric and adult SMA Type 1-3 patients without any past medical history of liver disease, who were seen physically in clinic from 2020-2022, and who had received hepatic sonography or fibroscan, had their sonographic or fibroscan steatosis grade determined and clinical serum markers of liver synthetic function and liver damage done at around the time of ultrasound reviewed. Units for liver enzymes are IU/L. Albumin, protein and bilirubin are in g/L. **Bold** – abnormal values.

a – upper limits of normal. Values more than 2-fold the upper limit of normal is considered abnormal [83]; b – patient was on phenobarbital; c – patient had a Body Mass Index (BMI) of 50.7; d - patient had a history of possible heavy alcohol use (not confirmed).

Table 2. Details of SMA hiPSCs

hiPSC Name	ID Number	*SMN1* Copy Number	*SMN2* Copy Number	SMA Type	Age Biopsy (Years)
1-49A	1049	0	4	III	28.4
1-56	1056	0	3	III	14.7
1-54B	1054	0	3	III	14.3
1-51N	1051	0	3	II	0.9
1-33L	1033	0	3	I	0.7
1-38G	1038	0	2	I	1.6
1-53F	1053	0	3	I	1.1
SMA15	SMA15	0	0	0	N/A

Table 3. CRISPR-edited 1-38G hiPSCs

Classification	hiPSC Name	Copies of *SMN2* edited to *SMN1*	*SMN2* Copy Number	*SMN1-like* Copy Number
Isogenic WT	HOM1, HOM2, HOM3	2	0	2
Isogenic Carrier	HET1, HET2, HET3	1	1	1